

# Set-membership target search and tracking within an unknown cluttered area using cooperating UAVs equipped with vision systems

Maxime Zagar\*, Luc Meyer\*\*, Michel Kieffer\* and H el ene Piet-Lahanier\*\*

**Abstract**—This paper addresses the problem of target search and tracking using a fleet of cooperating UAVs evolving in some unknown region of interest containing an *a priori* unknown number of moving ground targets. Each drone is equipped with an embedded Computer Vision System (CVS), providing an image with labeled pixels and a depth map of the observed part of its environment. Moreover, a box containing the corresponding pixels in the image frame is available when a UAV identifies a target. Hypotheses regarding information provided by the pixel classification, depth map construction, and target identification algorithms are proposed to allow its exploitation by set-membership approaches. A set-membership target location estimator is developed using the information provided by the CVS. Each UAV evaluates sets guaranteed to contain the location of the identified targets and a set possibly containing the locations of targets still to be identified. Then, each UAV uses these sets to search and track targets cooperatively.

**Index Terms**—MPC, Computer vision system, Cooperative target search and tracking, Set-membership

## I. INTRODUCTION

THE problem of searching and tracking targets using a fleet of Unmanned Aerial Vehicles (UAVs) in some Region of Interest (RoI) has attracted considerable attention in recent years, see, *e.g.*, [44], [41], [1], [31] and the references therein. The difficulty of this problem depends (*i*) on the knowledge available on the environment and on whether it is structured or not, (*ii*) on the type and quality of information provided by the sensors embedded in the UAVs, and (*iii*) on the *a priori* knowledge about targets (shape, number, dynamics).

Cooperative Search, Acquisition, and Track (CSAT) problems in possibly unknown and cluttered environments are still challenging [31]. In absence of prior knowledge about the environment, its representation is usually constructed in parallel to the search for targets [26], [22] using techniques like in [40]. For that purpose, UAVs must be equipped with a Computer Vision System (CVS) including a camera and image processing algorithms. Many prior works assume that a UAV gets a noisy measurement of the state of targets present in its FoV [24], [62], [59], [19], [56]. The complex processing performed by the CVS to get the state measurement from data acquired by the camera is ignored in these works. As a consequence, the estimation uncertainty associated to the state

measurements is difficult to characterize, and is thus roughly approximated, which is a major limit of those approaches.

This paper presents a CSAT approach for ground targets evolving in a structured environment for which no prior map is available. UAVs embed a CVS consisting of a camera with a limited Field of View (FoV), a pixel classifier, a depth map evaluation algorithm, and a target detection algorithm. Hypotheses are introduced regarding the information these algorithms provide to facilitate their processing by the UAVs. A distributed set-membership estimation approach is proposed to exploit the information provided by the CVS and to obtain sets containing the locations of identified targets compliant with the considered hypotheses. A set containing all locations of targets still to be identified is also evaluated. CVS information is also exploited to build sets where there is no target. Each UAV exploits the information provided by its own CVS and then accounts for the information broadcast by its neighbors. The trajectory of each UAV of the fleet is then evaluated using the Model Predictive Control (MPC) of [18] so as to minimize the estimation uncertainty characterized by the size of the set estimates.

To the best of our knowledge, this paper presents the first approach to address a CSAT problem by a distributed set-membership approach exploiting directly information provided by a CVS. Its main contribution lies in the combination of the introduction of hypotheses to exploit the information provided by the CVS in a set-membership context and the consideration of an unknown structured environment where obstacles may hide targets. The performance of the proposed approach is evaluated via a simulation in a simplified urban environment using information provided by a realistic model of a CVS.

Section II introduces some related work. The CSAT problem is formulated in Section III after an description of models for the targets, the UAVs, and the CVS. The set-membership estimator is developed in Section V and in Section V. Section VI recalls the distributed MPC approach to design the guidance law of each UAV. Simulation results are provided in Section VII before drawing some conclusions and perspectives in Section VIII.

## II. RELATED WORKS

CSAT approaches using a fleet of UAVs require to find, identify, locate, and track a possibly unknown number of targets present in some RoI [41], [25], [31]. For that purpose, it is necessary to collect informative measurements allowing

\* Universit e Paris-Saclay, Centralesupelec, CNRS, L2S 91192, Gif-sur-Yvette, France first.name.last.name@l2s.centralesupelec.fr

\*\* DTIS, ONERA Universit e Paris-Saclay, Palaiseau, France first.name.last.name@onera.fr

to discriminate the zones where a target can be located from the zones free of targets. When a target has been identified and its location estimated, the UAVs must keep track of its trajectory while pursuing the exploration of the RoI. Therefore, the displacements of the UAVs result in a compromise between exploratory search and target tracking. Many approaches have been proposed to achieve parts of these various goals, fewer address all of them, especially in an unknown environment.

#### A. Representation of the RoI

The simplest description of a RoI is to assume the absence of any obstacle. In this context, search trajectories for a fleet of UAVs have been designed in [9], [16], [6]. Nevertheless, the target search efficiency of these approaches decreases in presence of occlusions due to obstacles, leading to possible non-detections.

To account for the presence of obstacles, the fleet of UAVs may either exploit some *a priori* known map of the environment or build a map during the exploration. Exploration in cluttered environment without any map has been considered in [51], where a swarm of robots is driven to a target emitting some signal while using an obstacle collision avoidance approach. When several possibly partly hidden target have to be found, [19] considers groups of UAVs, each observing a part of the RoI with complementary points of view. This limits the risk a target being occluded from all points of view and does not require building a map of the environment to localize the targets. The price to be paid is an increase of the size of the fleet. Using a known map, the UAV trajectories can be efficiently and accurately determined [52], [13], [62]. Occlusions of the FoV by obstacles may be taken into account, as in [33].

Many Simultaneous Localization and Mapping (SLAM) algorithms have been developed to build maps, see the survey [40]. The map may be represented by an occupancy grid [15], an OcTree [4], or a point cloud [57]. The availability of semantic information improves the mapping algorithms [5], [61], [58], [4], [46], for example to distinguish static and mobile objects as in [61]. In outdoor environment mapping, [58], [46] use semantic information to evaluate the traversability between two locations, *i.e.*, the possibility to reach one location from another. Nevertheless, 3D mapping and exploration of large outdoor environments is still challenging [40], especially for aerial vehicles due to their limited computational power. For example, the mapping of a city-scale environment with an occupancy grid raises storage issues. OcTree mapping may reduce this complexity as shown in [4], but their study is limited to a ground exploration of areas of  $150 \text{ m} \times 150 \text{ m}$ .

CSAT algorithms including map construction during exploration have been considered in [26], [22]. These approaches consider either a 2D [22] or a 3D [26] description of the RoI, but neglect potential occlusions of the FoV by obstacles in the trajectory design.

#### B. Environment perception and target detection

Environment exploration, target detection, and map building heavily relies on the information provided by the UAV

sensors, such as images provided by cameras or depth measurements obtained either from LiDARs, or by processing the acquired images [39], [21], [32], [47]. Several computer vision algorithm may then be exploited such as image or point cloud segmentation [14], [17], [34]. Target detection techniques [43], [36], [30], [23] may then be put at work.

Once a target has been detected, several approaches have been proposed to estimate its location. In [35], [52], [49], [53], [28], [27], images of an RGB camera are used to estimate the location of a target in a reference frame from its location in the images. These approaches exploit some specific pixel, generally belonging to a 2D bounding box containing the pixels associated to the target. The selection of the pixel most representative of the target location is often heuristic and may lead to relatively large localization errors, as evidenced in [10] when estimating the location of humans evolving in the overlapping FoVs of static cameras. In [?], images of ArUco markers with known positions are acquired by UAVs, processed by a CVS, and exploited by a set-membership approach to cooperatively estimate the pose of the UAVs. Deep learning techniques are now commonly used for target location estimation. For example, YOLO [43] is used to localize a human in an unknown environment present in the FoV of a UAV in [2]. When the target remains in the FoV, it is tracked via optical-flow techniques. In [29], YOLO exploits RGB images and depth information to detect and localize ArUco markers placed on objects. Using strong *a priori* information such as 3D models of the target shapes, deep learning algorithms exploiting images and depth information, are able to estimate the location and orientation of objects [5], [55], or vehicles [45], [11]. Nevertheless, these algorithms may provide erroneous estimates with errors difficult to characterize [37].

#### C. Representations of the target location estimates

To represent the estimated target locations, a probability map is often considered, which requires a spatial discretization of the RoI [13], [60]. Nevertheless, the performance of grid-based approaches heavily relies on the choice of the cell dimension, and extension to large RoI is an issue [40]. Alternative approaches such as [9], [6] combine a probability hypothesis density filter and random finite sets. Assuming a bounded measurement noise, set-membership techniques may be used as in [18] to get sets guaranteed to contain the actual locations of targets, provided that the hypotheses on the noise bounds are satisfied.

Determining parts of RoI free of targets may be very helpful in the exploration process to reduce the estimation uncertainty of target locations. The absence or presence of a target within an area monitored by a UAV depends on the capacity of the embedded CVS to detect the presence of a target [3], often represented by a probability of detection. Nevertheless, this probability is highly dependent on the observation conditions (UAV point of view, possible occlusions) as evidenced in [50] and [33]. Therefore, this probability is hard to characterize. Consequently, in most approaches a detection probability is introduced [3], [9], [26], [16], but its value is rarely justified.

Alternatively, deterministic, point-of-view dependent target detection conditions have been introduced in [19]. A target may be detected and identified only when it is observed from some set of point of views. The set of point of views may be deduced from a map of the environment, as in [42]. Alternatively, the UAVs may be organized to observe simultaneously parts of the RoI from a large variety of point of views.

#### D. Trade-off between exploration and tracking

When mobile targets outnumber the UAVs, the fleet cannot continuously observe all targets. Different approaches have been proposed to trade off environment exploration and target tracking. Pre-planned trajectories are used in [38], [54]. In [33], several next best viewpoints for each UAV are first identified using the approach of [48], [15]. Then, polynomial trajectories are designed passing through these viewpoints while avoiding known obstacles. A potential-field based path-planning approach is developed in [26] to reach a location in a 3D cluttered environment. The goal location is a cell that characterized by a higher uncertainty about the presence of a target than other cells. Each UAV deployed by [9] updates its trajectory with new weighted center of Voronoi cells obtained once the random finite sets describing the possible target locations are updated. Trajectories are designed in [2], [16], [56] via reinforcement learning techniques. A MPC approach is used in [18] to design UAV trajectories minimizing the predicted estimation uncertainty corresponding to the area of the set estimates related to identified targets and of the set still to be explored.

#### E. Conclusion

This paper aims to propose an all-in-one approach to solve a CSAT problem in unknown cluttered environment by exploiting the real CVS information along set-membership techniques. Compared to other previous approaches, we propose a target location estimator which accounts for the most of the information provided by the CVS after the processing of measurement collected by embedded sensors. Our noise assumption relies on the quality of the sensors as well as the confidence we have on the chosen image processing algorithms to assess the presence of a target, detect the presence of an obstacles, or identify regions of the RoI where no useful conclusion can be made. Once the set-estimates gathering the potential target locations are updated from these CVS information, a cooperative Model Predictive Control (MPC) based on the work of [18] is used to update the guidance law of each UAV. Lastly, and to the best of our knowledge, the algorithm proposed in this article is the first to solve a CSAT problem with set-membership approaches using real CVS.

### III. HYPOTHESES, MODELS, AND PROBLEM FORMULATION

Consider an environment to which a frame  $\mathcal{F}$  is attached. Our RoI  $\mathbb{X}_0 \subset \mathbb{R}^2 \times \mathbb{R}^+$  is a subset of the environment and its ground  $\mathbb{X}_g$  is assumed to be flat, *i.e.*,  $\mathbb{X}_g = \{\mathbf{x} \in \mathbb{X}_0 \mid x_3 = 0\}$ .  $N^o$  static obstacles are spread within  $\mathbb{X}_0$ , with  $N^o$  unknown.

$\mathbb{S}_m^o$  denotes the unknown space occupied by the obstacle,  $m \in \mathcal{N}^o = \{1, \dots, N^o\}$ .

A fleet of  $N^u$  UAVs with indexes in the set  $\mathcal{N}^u = \{1, \dots, N^u\}$  is deployed in the RoI. The UAVs search a fixed but unknown number  $N^t$  of ground targets with indexes in the set  $\mathcal{N}^t = \{1, \dots, N^t\}$ . We assume that the targets never leave  $\mathbb{X}_0$  nor enter in any obstacle.

The time is sampled with a period  $T$  and  $k$  refers to the time index.

In what follows, several frames will be introduced, such as the frames attached to the UAVs. To lighten the notations, vectors with no superscript related to a frame are implicitly expressed in  $\mathcal{F}$ .

Section III-A introduces the model and assumptions considered for our targets and Section III-B presents the UAV model. Then, Section III-C introduces the geometrical model for the embedded camera and Section III-D presents our approach to interpret the information provided by the CVS. Section III-E adds an observation condition between the UAVs and the targets. Section III-F introduces the communication graph between UAVs. Finally, Section III-G formulates how we will address our problem.

#### A. Target model

At time  $t_k = kT$ , the state of target  $j \in \mathcal{N}^t$  is  $\mathbf{x}_{j,k}^t$ . The vector  $\mathbf{x}_{j,k}^t$  containing the first three components of  $\mathbf{x}_{j,k}^t$  gathers the coordinates of the center of gravity of target  $j$ . The projection of  $\mathbf{x}_{j,k}^t$  on  $\mathbb{X}_g$ , denoted as

$$\mathbf{x}_{j,k}^{t,g} = \mathbf{p}_g(\mathbf{x}_{j,k}^t), \quad (1)$$

corresponds to the target location at time  $t_k$ . A dynamical model of the evolution of  $\mathbf{x}_{j,k}^{t,g}$  is assumed to be available as

$$\mathbf{x}_{j,k+1}^{t,g} = \mathbf{f}^t(\mathbf{x}_{j,k}^{t,g}, \mathbf{v}_{j,k}^t), \quad (2)$$

where  $\mathbf{f}^t$  is known and  $\mathbf{v}_{j,k}^t$  represents the unknown but bounded target control input as well as the state perturbations only assumed to belong to a known box  $[\mathbf{v}^t]$ . The space occupied by target  $j$  is the subset  $\mathbb{S}_j^t(\mathbf{x}_{j,k}^t)$  of  $\mathbb{X}_0$  and depends on  $\mathbf{x}_{j,k}^t$ . When the target shape is rigid, *e.g.*, for cars,  $\mathbb{S}_j^t(\mathbf{x}_{j,k}^t)$  depends mainly on the target position and orientation. We assume that

$$\mathbf{x}_{j,k}^t \in \mathbb{S}_j^t(\mathbf{x}_{j,k}^t). \quad (3)$$

The target location  $\mathbf{x}_{j,k}^{t,g}$ , however, does not necessarily belong to  $\mathbb{S}_j^t(\mathbf{x}_{j,k}^t)$ , as in the case of cars, for example.

Usually, the type of targets to be localized is known. Consequently, some information about the target dimensions are available. We assume that a vertical circular right cylinder  $\mathbb{C}^t(\mathbf{x}_{j,k}^{t,g})$  of known height  $h^t$  and radius  $r^t$  with basis centered in  $\mathbf{x}_{j,k}^{t,g}$  can be defined such that, for any target state  $\mathbf{x}_{j,k}^t$ ,

$$\mathbb{S}_j^t(\mathbf{x}_{j,k}^t) \subset \mathbb{C}^t(\mathbf{x}_{j,k}^{t,g}). \quad (4)$$

The projection  $\mathbf{p}_g(\mathbb{C}^t(\mathbf{x}_{j,k}^{t,g}))$  of  $\mathbb{C}^t(\mathbf{x}_{j,k}^{t,g})$  on  $\mathbb{X}_g$  is the disc of center  $\mathbf{x}_{j,k}^{t,g}$  and radius  $r^t$ .

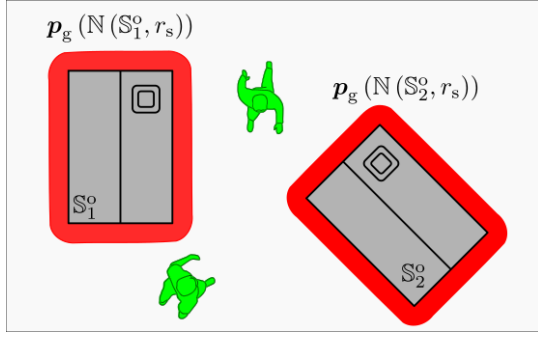


Fig. 1. Illustration of the  $r_s$ -neighborhood (in red) of two obstacles (in black). Targets are in green.

Consider the  $r_s$ -neighborhood of a set  $\mathbb{S} \subset \mathbb{X}_0$  as

$$\mathbb{N}(\mathbb{S}, r_s) = \{\mathbf{x} \in \mathbb{X}_0 \mid d(\mathbf{x}, \mathbb{S}) \leq r_s\} \quad (5)$$

with

$$d(\mathbf{x}, \mathbb{S}) = \min_{\mathbf{y} \in \mathbb{S}} \|\mathbf{x} - \mathbf{y}\|. \quad (6)$$

We assume that the distance between targets and obstacles is always larger than a safety distance  $r_s$ , *i.e.*,

$$\forall j \in \mathcal{N}^t, \forall m \in \mathcal{N}^o, \mathbb{S}_{j,k}^t(\mathbf{x}_{j,k}^t) \cap \mathbb{N}(\mathbb{S}_m^o, r_s) = \emptyset. \quad (7)$$

We assume moreover that a target cannot go under or over an obstacle. Combined with (7), this assumption leads to

$$\forall j \in \mathcal{N}^t, \forall m \in \mathcal{N}^o, \mathcal{P}_{\mathbb{S}_{j,k}^t(\mathbf{x}_{j,k}^t)} \cap \mathcal{P}_{\mathbb{N}(\mathbb{S}_m^o, r_s)} = \emptyset. \quad (8)$$

### B. UAV model

At time  $t_k$ , the state vector  $\mathbf{x}_{i,k}^u$  of UAV  $i \in \mathcal{N}^u$  contains, among others, the location of its center of gravity  $\mathbf{x}_{i,k}^u \in \mathbb{R}^2 \times \mathbb{R}^{+*}$ . The space occupied by UAV  $i$  is  $\mathbb{S}^u(\mathbf{x}_{i,k}^u)$  and its dynamics is modeled as

$$\mathbf{x}_{i,k+1}^u = \mathbf{f}_k^u(\mathbf{x}_{i,k}^u, \mathbf{u}_{i,k}^u), \quad (9)$$

where  $\mathbf{f}_k^u$  is known and the control input  $\mathbf{u}_{i,k}^u$  is constrained within a bounded set. The state  $\mathbf{x}_{i,k}^u$  is assumed to be perfectly known by UAV  $i$ . A body frame  $\mathcal{F}_i^b$ , illustrated in Figure 2, with origin  $\mathbf{x}_{i,k}^u$  is attached to UAV  $i$ . The rotation matrix from  $\mathcal{F}_i^b$  to  $\mathcal{F}$  is denoted  $\mathbf{M}_{\mathcal{F}_i^b}^{\mathcal{F}}$ . The coordinates of some vector  $\mathbf{x} \in \mathbb{R}^3$ , when expressed in  $\mathcal{F}_i^b$ , are

$$\mathbf{T}_{\mathcal{F}}^{\mathcal{F}_i^b}(\mathbf{x}) = \mathbf{M}_{\mathcal{F}_i^b}^{\mathcal{F}}(\mathbf{x} - \mathbf{x}_{i,k}^u). \quad (10)$$

In the remainder of this section, the time index  $k$  is omitted to lighten the notations.

### C. Camera model and field of view

Each UAV of the fleet embeds the same type of CCD camera which provides an image  $\mathbf{I}_i$  of  $N_r$  rows and  $N_c$  columns. The camera frame  $\mathcal{F}_i^c$  of UAV  $i$  has its optical center  $\mathbf{x}_i^{c, \mathcal{F}_i^b}$  as origin and is oriented such that the positive  $z$ -axis represents the optical axis of the camera. The  $x$ -axis is parallel to the

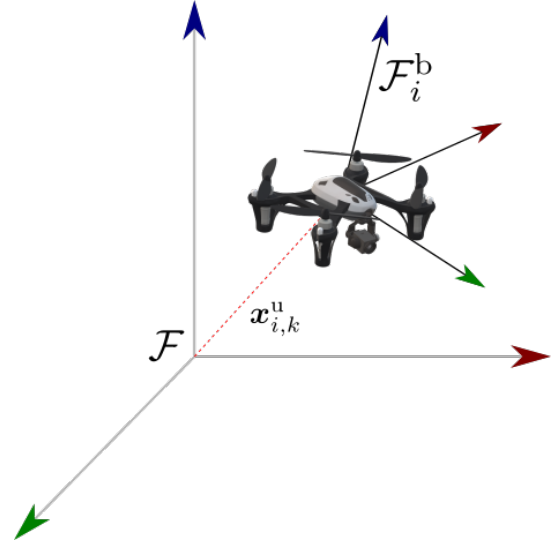


Fig. 2. Reference frame  $\mathcal{F}$  and UAV body frame  $\mathcal{F}_i^b$

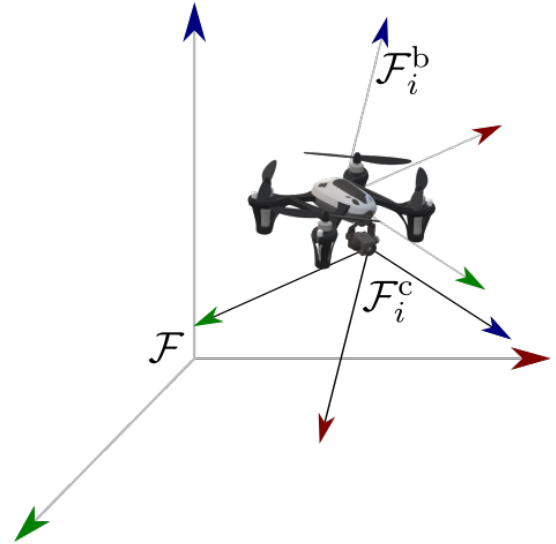


Fig. 3. Camera frame  $\mathcal{F}_i^c$  and body frame  $\mathcal{F}_i^b$  of UAV  $i$ , when  $\theta = 0$

pixel rows in the CCD array and the  $y$ -axis is parallel to the columns. The rotation matrix from  $\mathcal{F}_i^b$  to  $\mathcal{F}_i^c$  is

$$\mathbf{M}_{\mathcal{F}_i^b}^{\mathcal{F}_i^c} = \begin{pmatrix} 0 & -1 & 0 \\ 0 & 0 & -1 \\ 1 & 0 & 0 \end{pmatrix} \begin{pmatrix} \cos \theta & 0 & -\sin \theta \\ 0 & 1 & 0 \\ \sin \theta & 0 & \cos \theta \end{pmatrix}, \quad (11)$$

where  $\theta$  is the fixed camera angle between the  $x$ -axis of  $\mathcal{F}_i^b$  and the  $z$ -axis of  $\mathcal{F}_i^c$ . Figure 3 illustrates these two frames.

The dimensions  $H_r \times H_c$  of the CCD array of the camera and its focal length  $f$  are known. A pinhole model without distortion [12] is considered for the camera. Therefore, the matrix of intrinsic parameters [12] used to project a point of  $\mathcal{F}_i^c$  onto the CCD array is

$$\mathbf{K} = \begin{pmatrix} -f_c & 0 & N_c/2 \\ 0 & -f_r & N_r/2 \end{pmatrix} \quad (12)$$

where  $f_c = fN_c/H_c$  and  $f_r = fN_r/H_r$  are the focal lengths expressed in pixels.

Consequently, the 2D coordinates on the CCD array of the projection of some point  $\mathbf{x}^{\mathcal{F}_i^c} \in \mathbb{R}^3$  are

$$\mathbf{p}_{\mathcal{F}_i^c}(\mathbf{x}^{\mathcal{F}_i^c}) = \mathbf{K}\mathbf{x}^{\mathcal{F}_i^c}/x_3^{\mathcal{F}_i^c}. \quad (13)$$

According to the considered pinhole model, each light ray passing through the optical center of the camera and illuminating the CCD array at  $(x, y) \in [0, N_c] \times [0, N_r]$  can be modeled by a half-line of direction

$$\mathbf{v}^{\mathcal{F}_i^c}(x, y) = \frac{1}{\nu(x, y)} \begin{pmatrix} \left(\frac{N_c}{2} - x\right)/f_c \\ \left(\frac{N_r}{2} - y\right)/f_r \\ 1 \end{pmatrix}, \quad (14)$$

with

$$\nu(x, y) = \sqrt{\left(\left(\frac{N_c}{2} - x\right)/f_c\right)^2 + \left(\left(\frac{N_r}{2} - y\right)/f_r\right)^2 + 1}. \quad (15)$$

The set

$$\mathcal{V}_i(n_r, n_c) = \left\{ \mathbf{M}_{\mathcal{F}_i^c}^{\mathcal{F}_i^c} \mathbf{v}^{\mathcal{F}_i^c}(x, y) \mid x \in [n_c - 1, n_c], y \in [n_r - 1, n_r] \right\}, \quad (16)$$

with  $\mathbf{M}_{\mathcal{F}_i^c}^{\mathcal{F}_i^c} = \mathbf{M}_{\mathcal{F}_i^b}^{\mathcal{F}_i^c} \mathbf{M}_{\mathcal{F}_i^c}^{\mathcal{F}_i^b}$  contains the directions, expressed in  $\mathcal{F}_i^c$ , of all light rays contributing to the illumination of the pixel  $(n_r, n_c)$ .

The Field of View (FoV)  $\mathbb{F}(\mathbf{x}_i^u)$  of the CCD camera of UAV  $i$  (dubbed as FoV of UAV  $i$  in what follows) represents the set of points in  $\mathbb{X}_0$  that are potentially observed (ignoring obstacles and targets).  $\mathbb{F}(\mathbf{x}_i^u)$  is a half-cone with the camera optical center  $\mathbf{x}_i^c$  as its apex and with four unit vectors  $\mathbf{v}_\ell^{\mathcal{F}_i^c}$ ,  $\ell = 1, \dots, 4$ , describing its edges, *i.e.*,

$$\mathbb{F}(\mathbf{x}_i^u) = \left\{ \mathbf{x}_i^c + \sum_{\ell=1}^4 a_\ell \mathbf{M}_{\mathcal{F}_i^c}^{\mathcal{F}_i^c} \mathbf{v}_\ell^{\mathcal{F}_i^c} \mid a_\ell \in \mathbb{R}^+ \right\}. \quad (17)$$

Those four unit vectors can be deduced from (14) by taking  $(x, y)$  at the four corners of the CCD array. In what follows, we assume that any information related to some  $\mathbf{x} \in \mathbb{F}(\mathbf{x}_i^u)$  at a distance from  $\mathbf{x}_i^c$  larger than  $d_{\max}$  cannot be considered as reliable. One introduces then the following subset of the FoV

$$\underline{\mathbb{F}}(\mathbf{x}_i^u) = \mathbb{F}(\mathbf{x}_i^u) \cap \mathbb{B}(\mathbf{x}_i^c, d_{\max}), \quad (18)$$

where  $\mathbb{B}(\mathbf{x}_i^c, d_{\max})$  is the ball of  $\mathbb{R}^3$  of center  $\mathbf{x}_i^c$  and radius  $d_{\max}$ .

In what follows, we express the coordinates on the CCD array of a point  $\mathbf{x} \in \mathbb{F}(\mathbf{x}_i^u)$ . Its coordinates, when expressed in  $\mathcal{F}_i^b$  are  $\mathbf{x}^{\mathcal{F}_i^b} \in \mathbb{R}^3$ . To express them in  $\mathcal{F}_i^c$ , one evaluates

$$\mathbf{T}_{\mathcal{F}_i^c}^{\mathcal{F}_i^b}(\mathbf{x}^{\mathcal{F}_i^b}) = \mathbf{M}_{\mathcal{F}_i^c}^{\mathcal{F}_i^b}(\mathbf{x}^{\mathcal{F}_i^b} - \mathbf{x}_i^c, \mathcal{F}_i^b). \quad (19)$$

Composing (10) and (19), one gets the transform

$$\mathbf{T}_{\mathcal{F}_i^c}^{\mathcal{F}_i^u} = \mathbf{T}_{\mathcal{F}_i^c}^{\mathcal{F}_i^b} \circ \mathbf{T}_{\mathcal{F}_i^b}^{\mathcal{F}_i^u} \quad (20)$$

to express the coordinates of  $\mathbf{x} \in \mathbb{F}(\mathbf{x}_i^u)$  in  $\mathcal{F}_i^c$ .

Combining (13) and (20), the coordinates in the CCD array of a point  $\mathbf{x} \in \mathbb{F}(\mathbf{x}_i^u)$  are

$$\mathbf{p}_c(\mathbf{x}_i^u, \mathbf{x}) = \mathbf{p}_{\mathcal{F}_i^c}(\mathbf{T}_{\mathcal{F}_i^c}^{\mathcal{F}_i^u}(\mathbf{x})). \quad (21)$$

The notation  $\mathbf{p}_c(\mathbf{x}_i^u, \mathbf{x}) \in (n_r, n_c)$ , with  $\mathbf{x} \in \mathbb{F}(\mathbf{x}_i^u)$ , indicates that the projection of  $\mathbf{x}$  on the camera image belongs to the

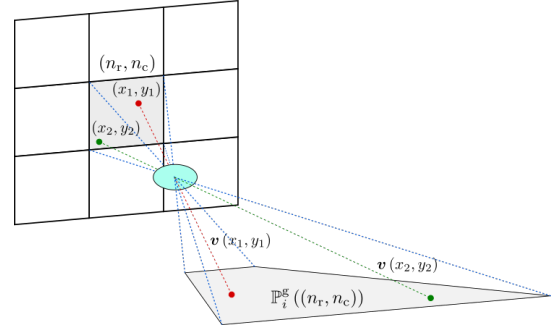


Fig. 4. Pinhole model of the camera and several light rays (green, red and blue) contributing to the illumination of the pixel  $(n_r, n_c)$  highlighted in gray. The 4 blue lines are the light rays illuminating the corners of  $(n_r, n_c)$ . The quadrangle  $\mathbb{P}_i^c((n_r, n_c))$  is defined in section IV.

pixel with coordinates  $(n_r, n_c) \in \mathcal{N}^1$ , with  $\mathcal{N}^1 = \{1 \dots N_r\} \times \{1 \dots N_c\}$ . Consequently, one has

$$\mathbf{x} \in \mathbb{F}(\mathbf{x}_i^u) \Rightarrow \exists (n_r, n_c) \in \mathcal{N}^1, \mathbf{p}_c(\mathbf{x}_i^u, \mathbf{x}) \in (n_r, n_c). \quad (22)$$

#### D. Exploiting information provided by the CVS

This section presents the assumptions considered to exploit the information provided by the CVS embedded in each UAV. In addition to the acquired image  $\mathbf{I}_i$ , the CVS provides a depth-map  $\mathbf{D}_i$  obtained using, *e.g.*, [39], [32], [47], an array of pixel labels  $\mathbf{L}_i$  obtained using, *e.g.*, [14], [17], and a list  $\mathcal{D}_i^t$  of identified targets. For each of these targets, a box  $[\mathcal{Y}_{i,j}^t]$  in the image  $\mathbf{I}_i$  containing pixels of the identified targets  $j \in \mathcal{D}_i^t$  may be provided, *e.g.*, by [43], [36], [30], [23]. We assume also that a CVS provides a depth map  $\mathbf{D}_i$  and an array of labels  $\mathbf{L}_i$ , both of the same size as  $\mathbf{I}_i$ .

Section III-D1 introduces an hypothesis on the information in  $\mathbf{D}_i$  to get bounded-error distance measurements to parts of the environment. Section III-D2 illustrates how to convert a pixel label into an exploitable information. Section III-D3 presents an assumption to associate  $\mathbf{L}_i$  with the boxes provided by the CVS.

1) *From a depth map to bounded-error range measurements:* The distance between the optical center of the camera  $\mathbf{x}_i^c$  and the environment (including obstacles and targets) along  $\mathbf{v} \in \mathcal{V}_i(n_r, n_c)$ , for any  $(n_r, n_c) \in \mathcal{N}^1$ , is

$$\rho(\mathbf{x}_i^c, \mathbf{v}) = \min \left\{ d_v(\mathbf{x}_i^c, \mathbb{X}_g), d_v\left(\mathbf{x}_i^c, \bigcup_{m \in \mathcal{N}^o} \mathbb{S}_m^o\right), \quad (23)$$

$$d_v\left(\mathbf{x}_i^c, \bigcup_{j \in \mathcal{N}^t} \mathbb{S}_j^t(\mathbf{x}_j^t)\right), d_v\left(\mathbf{x}_i^c, \bigcup_{\ell \in \mathcal{N}^u} \mathbb{S}^u(\mathbf{x}_\ell^u)\right) \right\},$$

where  $d_v(\mathbf{x}, \mathbb{S})$  is the distance from a point  $\mathbf{x} \in \mathbb{X}_0$  to the intersection of the set  $\mathbb{S}$  along the half-line of origin  $\mathbf{x}$  and direction  $\mathbf{v}$ . Then

$$\rho(\mathbf{x}_i^c, \mathcal{V}_i(n_r, n_c)) = \{\rho(\mathbf{x}_i^c, \mathbf{v}) \mid \mathbf{v} \in \mathcal{V}_i(n_r, n_c)\}, \quad (24)$$

is the set of all distances between  $\mathbf{x}_i^c$  and the environment along any direction  $\mathbf{v} \in \mathcal{V}_i(n_r, n_c)$ .

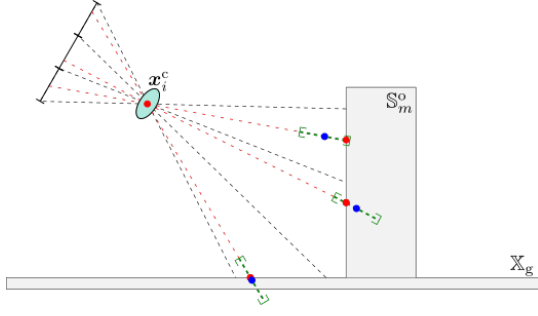


Fig. 5. Exploitation of the depth map information for three different pixels:  $\mathbf{D}_i^0(n_r, n_c)$  is the distance between  $\mathbf{x}_i^c$  and the red dots, while  $\mathbf{D}_i(n_r, n_c)$  represents the measured distance between  $\mathbf{x}_i^c$  and the blue dots. The green interval is  $[\mathbf{D}_i](n_r, n_c)$ .

We assume that each element  $\mathbf{D}_i(n_r, n_c)$  of the depth map is a noisy version

$$\mathbf{D}_i(n_r, n_c) = \mathbf{D}_i^0(n_r, n_c)(1 + w) \quad (25)$$

of the distance  $\mathbf{D}_i^0(n_r, n_c) = \rho(\mathbf{x}_i^c, \mathbf{v})$  between  $\mathbf{x}_i^c$  and the environment along some unknown direction  $\mathbf{v} \in \mathcal{V}_i(n_r, n_c)$ . In (25), the noise  $w$  is assumed to belong to the known interval  $[\underline{w}, \bar{w}]$ . Consequently, the interval

$$[\mathbf{D}_i](n_r, n_c) = \left[ \frac{1}{1 + \bar{w}}, \frac{1}{1 + \underline{w}} \right] \mathbf{D}_i(n_r, n_c). \quad (26)$$

contains  $\mathbf{D}_i^0(n_r, n_c)$ .

2) *Classifier*: Each element  $(n_r, n_c)$  of the array of labels  $\mathbf{L}_i$  is assumed to belong to one of the following classes: Ground, Target, Obstacle, and Unknown/Not Labeled. The latter class corresponds to pixels that cannot be classified in one of the three other classes due to a lack of confidence. According to (18), all information coming from a point that may not be in  $\mathbb{F}(\mathbf{x}_i^u)$  is considered as unreliable. Therefore, using  $\mathbf{D}_i$ , one characterizes the list

$$\mathcal{Y}_i = \left\{ (n_r, n_c) \in \mathcal{N}^t \mid \frac{1}{1 + \underline{w}} \mathbf{D}_i(n_r, n_c) \leq d_{\max} \right\} \quad (27)$$

of pixel coordinates for which reliable information is assumed available, especially about their labeling. Consequently, all pixels with indexes in  $\mathcal{Y}_i$  are assumed to be correctly classified (possibly as Unknown, when there is an ambiguity).

Four subsets of  $\mathcal{Y}_i$  are then deduced from  $\mathbf{L}_i$ , namely  $\mathcal{Y}_i^g$ ,  $\mathcal{Y}_i^t$ ,  $\mathcal{Y}_i^o$ , and  $\mathcal{Y}_i^n$  gathering coordinates of pixels respectively labeled as Ground, Target, Obstacle, and Unknown/Not Labeled. We assume that pixels corresponding to other UAVs are labeled as Unknown.

Moreover, we assume that if a pixel  $(n_r, n_c) \in \mathcal{Y}_i^g$ , then all light rays illuminating pixel  $(n_r, n_c)$  stem from the ground  $\mathbb{X}_g$ , i.e.,

$$\forall \mathbf{v} \in \mathcal{V}_i(n_r, n_c), \rho(\mathbf{x}_i^u, \mathbf{v}) = d_v(\mathbf{x}_i^c, \mathbb{X}_g). \quad (28)$$

Similarly, if a pixel  $(n_r, n_c) \in \mathcal{Y}_i^t$ , then there exists a target  $j \in \mathcal{N}^t$  such that all light rays illuminating pixel  $(n_r, n_c)$  stem from  $\mathbb{S}_j^t(\mathbf{x}_{j,k}^t)$ , i.e.,

$$\forall \mathbf{v} \in \mathcal{V}_i(n_r, n_c), \exists j \in \mathcal{N}^t, \rho(\mathbf{x}_i^u, \mathbf{v}) = d_v(\mathbf{x}_i^c, \mathbb{S}_j^t(\mathbf{x}_{j,k}^t)). \quad (29)$$

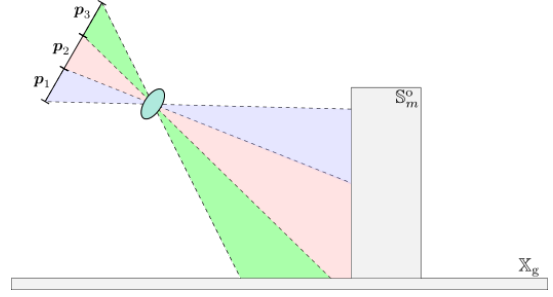


Fig. 6. As pixel  $p_1 \in \mathcal{Y}_i^o$ , all light rays illuminating  $p_1$  stem from an obstacle; as pixel  $p_3 \in \mathcal{Y}_i^g$ , all light rays illuminating  $p_3$  stem from  $\mathbb{X}_g$ ; As  $p_2 \in \mathcal{Y}_i^n$ , nothing can be concluded.

Finally, if a pixel  $(n_r, n_c) \in \mathcal{Y}_i^o$ , then there exists an obstacle  $m \in \mathcal{N}^o$  such that all light rays illuminating pixel  $(n_r, n_c)$  stem from  $\mathbb{S}_m^o$ , i.e.,

$$\forall \mathbf{v} \in \mathcal{V}_i(n_r, n_c), \exists m \in \mathcal{N}^o, \rho(\mathbf{x}_i^u, \mathbf{v}) = d_v(\mathbf{x}_i^c, \mathbb{S}_m^o). \quad (30)$$

3) *Target detection and identification*: When  $\mathcal{Y}_i^t$  is not empty, at least one target located within  $\mathbb{F}(\mathbf{x}_i^u)$  has been detected. In such case, the CVS may also provide a list  $\mathcal{D}_i^t \subset \mathcal{N}^t$  of targets identified and an axis-aligned box  $[\mathcal{Y}_{i,j}^t]$ , for each  $j \in \mathcal{D}_i^t$ .  $\mathcal{D}_i^t$  may be empty even if  $\mathcal{Y}_i^t$  is not empty, because  $\mathcal{Y}_i^t$  contains not enough information to allow any target identification.

Consider the set  $\mathcal{Y}_{i,j}^t \subset \mathcal{Y}_i^t$  containing all pixels of  $\mathcal{Y}_i^t$  associated to target  $j$  only.. If  $\mathcal{D}_i^t$  is not empty and  $j \in \mathcal{D}_i^t$ , we assume that  $\mathcal{Y}_{i,j}^t$  is not empty, i.e.,

$$j \in \mathcal{D}_i^t \Rightarrow \mathcal{Y}_{i,j}^t \neq \emptyset. \quad (31)$$

Moreover, the CVS is assumed to be tuned in such a way that  $[\mathcal{Y}_{i,j}^t]$  contains  $\mathcal{Y}_{i,j}^t$ , i.e.,

$$j \in \mathcal{D}_i^t \Rightarrow \mathcal{Y}_{i,j}^t \subset [\mathcal{Y}_{i,j}^t]. \quad (32)$$

In addition to pixels in  $\mathcal{Y}_{i,j}^t$ , the axis-aligned box  $[\mathcal{Y}_{i,j}^t]$  usually also contains pixels belonging to  $\mathcal{Y}_i^g$ ,  $\mathcal{Y}_i^o$ , or  $\mathcal{Y}_i^t \setminus \mathcal{Y}_{i,j}^t$ . We assume that the classifier is unable to provide  $\mathcal{Y}_{i,j}^t$ . Therefore, the target location estimator will have to exploit  $[\mathcal{Y}_{i,j}^t]$  and  $\mathcal{Y}_i^t$  only.

#### E. Assumption on observed targets

Consider some target  $j$  such that  $\mathbf{x}_j^{\text{t;g}} \in \mathbb{F}(\mathbf{x}_i^u)$ . We assume that the half-open segment  $[\mathbf{x}_i^c, \mathbf{x}_j^{\text{t;g}}[$  intersects  $\mathbb{S}_j^t(\mathbf{x}_j^t)$ , i.e.,

$$\mathbf{x}_j^{\text{t;g}} \in \mathbb{F}(\mathbf{x}_i^u) \Rightarrow [\mathbf{x}_i^c, \mathbf{x}_j^{\text{t;g}}[ \cap \mathbb{S}_j^t(\mathbf{x}_j^t) \neq \emptyset. \quad (33)$$

Thus, if  $\mathbf{x}_j^{\text{t;g}}$  belongs to the FoV, then some points on  $\mathbb{S}_j^t(\mathbf{x}_j^t)$  will reflect a light ray that will illuminate the CCD array of the camera (in absence of obstacles). Consequently, if  $\mathbf{x}_j^{\text{t;g}} \in \mathbb{F}(\mathbf{x}_i^u)$ , then there exists a pixel  $(n_r, n_c)$  such that  $\mathbf{p}_c(\mathbf{x}_i^u, \mathbf{x}_j^{\text{t;g}}) \in (n_r, n_c)$ . Then according to (33) and (28),  $(n_r, n_c) \notin \mathcal{Y}_i^g$ .

The assumption (33) is instrumental in the exploration process to characterize parts of  $\mathbb{X}_g$  that cannot contain any target location. The validity of this assumption depends on the camera orientation and on the characteristics of the shape



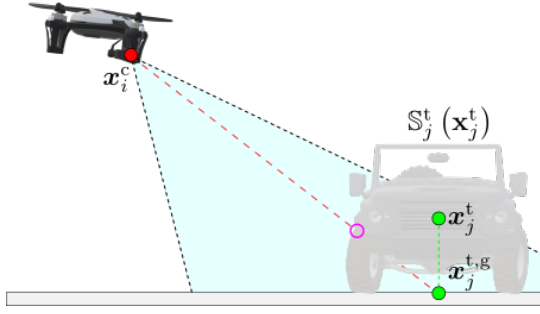


Fig. 7. Illustration of (33). The green dots represent respectively  $\mathbf{x}_{j,k}^t$  and  $\mathbf{x}_{j,k}^{t,g}$ . The dashed-red line is the line-of-sight  $[\mathbf{x}_{i,k}^c, \mathbf{x}_{j,k}^{t,g}]$ . The purple dot represents the part of  $\mathbb{S}_j^t(\mathbf{x}_j^t)$  seen by the UAV.

$\mathbb{S}_j^t(\mathbf{x}_j^t)$ . It is reasonable for many targets such as cars, trucks, provided that they are observed from a location sufficiently above the target, with a camera oriented towards the ground.

### F. Communications

The communications within the fleet are modeled by the undirected graph  $\mathcal{G}_k = (\mathcal{N}^u, \mathcal{E}_k)$ , with  $\mathcal{N}^u$  the set of vertices and  $\mathcal{E}_k = \mathcal{N}^u \times \mathcal{N}^u$  the set of edges of the graph.  $\mathcal{E}_k$  describes the connectivity at time  $t_k$ . For two UAVs  $i \in \mathcal{N}^u$  and  $i' \in \mathcal{N}^u$ , if  $(i, i') \in \mathcal{E}_k$ , then both UAVs are able to exchange information without delay and error. The set  $\mathcal{N}_{i,k} = \{i' \in \mathcal{N}^u \mid (i, i') \in \mathcal{E}_k\}$  contains all UAV indexes to which UAV  $i$  is able to communicate at time  $t_k$ . For simplicity, we consider that  $i \in \mathcal{N}_{i,k}$ .

### G. Problem formulation

Assume that the information available to UAV  $i$  before time  $t_k$  is gathered in the set  $\mathcal{I}_{i,k-1}$ .  $\mathcal{I}_{i,k-1}$  contains, among others, a list  $\mathcal{L}_{i,k-1}^t$  of identifiers of targets already identified. For each  $j \in \mathcal{L}_{i,k-1}^t$ , we assume that UAV  $i$  has access to a set estimate  $\mathbb{X}_{i,j,k-1}^t \subset \mathbb{X}_g$  of all possible target locations  $\mathbf{x}_{j,k-1}^{t,g}$  which are consistent with  $\mathcal{I}_{i,k-1}$ . It has also access to a set  $\bar{\mathbb{X}}_{i,k-1}^t$  containing all locations where targets still to be detected may be present.

At time  $t_k$ , UAV  $i$  has access to an image  $\mathbf{I}_{i,k}$ , a depth-map  $\mathbf{D}_{i,k}$ , and an array of labels  $\mathbf{L}_{i,k}$ . The embedded CVS may also provide a list  $\mathcal{D}_{i,k}^t$  of identified targets and a list  $\mathcal{B}_{i,k}^t = \left\{ [\mathcal{Y}_{i,j,k}^t] \right\}_{j \in \mathcal{D}_{i,k}^t}$  of associated bounding boxes. The information available at time  $t_k$  is then  $\mathcal{I}_{i,k|k} = \mathcal{I}_{i,k-1} \cup \left\{ \mathbf{I}_{i,k}, \mathbf{D}_{i,k}, \mathbf{L}_{i,k}, \mathcal{D}_{i,k}^t, \mathcal{B}_{i,k}^t \right\}$ . Using this information UAV  $i$  evaluates an updated list of identified targets  $\mathcal{L}_{i,k|k}^t = \mathcal{L}_{i,k-1}^t \cup \mathcal{D}_{i,k}^t$ . It has then, for each targets  $j \in \mathcal{L}_{i,k|k}^t$  to characterize the set  $\mathbb{X}_{i,j,k|k}^t \subset \mathbb{X}_g$  of all possible target locations  $\mathbf{x}_{j,k}^{t,g}$  which are consistent with  $\mathcal{I}_{i,k|k}$ . UAV  $i$  has also to update the estimate  $\bar{\mathbb{X}}_{i,k-1}^t$  to get  $\bar{\mathbb{X}}_{i,k|k}^t$ . Then, UAV  $i$  broadcasts some updated information to its neighbors  $\mathcal{N}_{i,k}$  and receives information from them. With this new information, UAV  $i$  has now access to  $\mathcal{I}_{i,k} = \mathcal{I}_{i,k|k} \cup \mathcal{I}_{i,k}^N$ , from which UAV  $i$  further updates its list of identified targets to get  $\mathcal{L}_{i,k}^t$ , the set estimates  $\mathbb{X}_{i,j,k}^t$

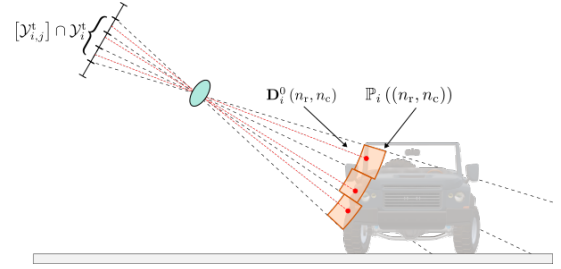


Fig. 8. Illustration of the sets  $\mathbb{P}_i((n_r, n_c))$  (in orange) for different  $(n_r, n_c) \in [\mathcal{Y}_{i,j}^t]$  and for a target detected and identified by UAV  $i$

for each  $j \in \mathcal{L}_{i,k}^t$ , which are gathered in  $\mathcal{X}_{i,k}^t$ , as well as an updated version of  $\bar{\mathbb{X}}_{i,k|k}^t$  denoted  $\bar{\mathbb{X}}_{i,k}^t$ .

We defined the estimated uncertainty about the localization of both identified and undetected targets as

$$\Phi(\mathcal{X}_{i,k}^t, \bar{\mathbb{X}}_{i,k}^t) = \phi\left(\bar{\mathbb{X}}_{i,k}^t \cup \bigcup_{j \in \mathcal{L}_{i,k}^t} \mathbb{X}_{i,j,k}^t\right), \quad (34)$$

with  $\phi(\mathbb{X})$  being the area of the surface  $\mathbb{X} \subset \mathbb{R}^2$ . Our aim is to design a control input for each UAV in order to minimize (34).

## IV. EXPLOITING CVS INFORMATION FOR SET-MEMBERSHIP ESTIMATION

Using the information provided by the CVS of UAV  $i$ , Section IV-A presents an approach to estimate the location of a target  $j$  identified at time  $t_k$ . Then, Section IV-B describes how the CVS information can be used to characterize a part of  $\mathbb{X}_g$  clear of any target. Section IV-C describes how to characterize the occluded area. In this section, the time index  $k$  is omitted to lighten notations.

Appendixes B and C describe more precisely how the set estimates introduced in this section may be computed.

### A. Estimation of the location of a target

To estimate the location  $\mathbf{x}_j^{t,g}$  of an identified target  $j \in \mathcal{D}_i^t$ , UAV  $i$  has access to the bounding box  $[\mathcal{Y}_{i,j}^t]$ , the indexes of pixels labeled as Target  $\mathcal{Y}_{i,j}^t$ , and the depth map  $\mathbf{D}_i$ . From these measurements related to target  $j$ , UAV  $i$  can characterize a set  $\mathbb{X}_{i,j}^{t,m}$  such that  $\mathbf{x}_j^{t,g} \in \mathbb{X}_{i,j}^{t,m}$ .

Consider a target  $j$  such that  $j \in \mathcal{D}_i^t$ . One will first characterize a subset of  $\mathbb{X}_0$  that has a non-empty intersection with  $\mathbb{S}_j^t(\mathbf{x}_j^t)$ . For that purpose, for each pixel  $(n_r, n_c) \in \mathbf{I}_i$ , consider the set

$$\mathbb{P}_i((n_r, n_c)) = \left\{ \mathbf{x} \in \mathbb{F}(\mathbf{x}_i^u) \cap \mathbb{X}_0 \mid \exists \mathbf{v} \in \mathcal{V}_i(n_r, n_c), d_{\mathbf{v}}(\mathbf{x}_i^c, \{\mathbf{x}\}) \in [\mathbf{D}_i](n_r, n_c) \right\} \quad (35)$$

of all points in  $\mathbb{F}(\mathbf{x}_i^u) \cap \mathbb{X}_0$  that may have contributed to the illumination of  $(n_r, n_c)$  while being at a distance from UAV  $i$  consistent with  $\mathbf{D}_i(n_r, n_c)$ , see Figure 8.

According to (31),  $\mathcal{Y}_{i,j}^t \neq \emptyset$ . Moreover, from (32), one has  $\mathcal{Y}_{i,j}^t \subset [\mathcal{Y}_{i,j}^t]$ . Nevertheless, as indicated in Section III-D3, only the set of pixels  $\mathcal{Y}_i^t$  such that  $\mathcal{Y}_{i,j}^t \subset \mathcal{Y}_i^t$  is available.

Proposition 1 states that there exists at least one pixel  $(n_r, n_c)$  in  $[\mathcal{Y}_{i,j}^t] \cap \mathcal{Y}_i^t$  for which the set  $\mathbb{P}_i((n_r, n_c))$  intersects  $\mathbb{S}_j^t(\mathbf{x}_j^t)$ .

*Proposition 1:* If  $j \in \mathcal{D}_i^t$ , then  $\exists (n_r, n_c) \in [\mathcal{Y}_{i,j}^t] \cap \mathcal{Y}_i^t$  such that  $\mathbb{P}_i((n_r, n_c)) \cap \mathbb{S}_j^t(\mathbf{x}_j^t) \neq \emptyset$ .

*Proof 2:* If  $j \in \mathcal{D}_i^t$ , then  $\mathcal{Y}_{i,j}^t \neq \emptyset$  and  $\mathcal{Y}_{i,j}^t \subset [\mathcal{Y}_{i,j}^t]$ . Combining (31), (32), and (29),  $\exists (n_r, n_c) \in [\mathcal{Y}_{i,j}^t] \cap \mathcal{Y}_i^t$  such that for all  $\mathbf{v} \in \mathcal{V}_i(n_r, n_c)$ ,  $\rho(\mathbf{x}_i^u, \mathbf{v}) = d_{\mathbf{v}}(\mathbf{x}_i^c, \mathbb{S}_j^t(\mathbf{x}_j^t))$ . Therefore,  $\exists \mathbf{v} \in \mathcal{V}_i(n_r, n_c)$  and  $\exists \mathbf{x} \in \mathbb{S}_j^t(\mathbf{x}_j^t)$  such that  $d_{\mathbf{v}}(\mathbf{x}_i^c, \{\mathbf{x}\}) = \mathbf{D}_i^0(n_r, n_c)$ . As  $(n_r, n_c) \in \mathcal{Y}_i^t \subset \mathcal{Y}_i$ , according to (27),  $\frac{1}{1+w} \mathbf{D}_i(n_r, n_c) \leq d_{\max}$  and  $d_{\mathbf{v}}(\mathbf{x}_i^c, \{\mathbf{x}\}) \leq d_{\max}$ . Therefore  $\mathbf{x} \in \mathbb{F}(\mathbf{x}_i^u)$ . Finally, from (35), we have  $\mathbf{x} \in \mathbb{P}_i((n_r, n_c))$ . So  $\mathbb{P}_i((n_r, n_c)) \cap \mathbb{S}_j^t(\mathbf{x}_j^t) \neq \emptyset$ .

According to Proposition 1, a pixel  $(n_r, n_c)$  such that  $\mathbb{P}_i((n_r, n_c)) \cap \mathbb{S}_j^t(\mathbf{x}_j^t) \neq \emptyset$  exists, but it is only known to belong to  $\mathcal{Y}_i^t \cap [\mathcal{Y}_{i,j}^t]$ . To get a set intersecting  $\mathbb{S}_j^t(\mathbf{x}_j^t)$ , one has then to consider the union of all sets  $\mathbb{P}_i((n_r, n_c))$  for the pixels  $(n_r, n_c) \in [\mathcal{Y}_{i,j}^t] \cap \mathcal{Y}_i^t$ , see Corollary 3, which is a direct consequence of Proposition 1.

*Corollary 3:* If  $j \in \mathcal{D}_i^t$ , then the set

$$\mathbb{P}_{i,j}^t = \bigcup_{(n_r, n_c) \in [\mathcal{Y}_{i,j}^t] \cap \mathcal{Y}_i^t} \mathbb{P}_i((n_r, n_c)) \quad (36)$$

is such that  $\mathbb{P}_{i,j}^t \cap \mathbb{S}_j^t(\mathbf{x}_j^t) \neq \emptyset$ .

Again,  $\mathbb{P}_{i,j}^t$  is only known to intersect  $\mathbb{S}_j^t(\mathbf{x}_j^t)$ . If  $\mathbf{x} \in \mathbb{P}_{i,j}^t \cap \mathbb{S}_j^t(\mathbf{x}_j^t)$  would be available, exploiting the fact that  $\mathbb{S}_j^t(\mathbf{x}_j^t) \subset \mathbb{C}^t(\mathbf{x}_j^{t,g})$ , one would have  $\mathbf{x}_j^{t,g} \in \mathbb{C}^t(\mathbf{p}_g(\mathbf{x}))$ , see Proposition 16 in Appendix A. Therefore, the set estimate  $\mathbb{X}_{i,j}^{t,m}$  of  $\mathbf{x}_j^{t,g}$  introduced in Proposition 4 accounts for the fact that  $\mathbf{x}$  is only known to belong to  $\mathbb{P}_{i,j}^t$ .

*Proposition 4:* If  $j \in \mathcal{D}_i^t$ , then the set estimate

$$\mathbb{X}_{i,j}^{t,m} = \mathbb{X}_g \cap \bigcup_{\mathbf{x} \in \mathbb{P}_{i,j}^t} \mathbb{C}^t(\mathbf{p}_g(\mathbf{x})) \quad (37)$$

is such that  $\mathbf{x}_j^{t,g} \in \mathbb{X}_{i,j}^{t,m}$ .

*Proof 5:* See Appendix A.

In practice, the estimate  $\mathbb{X}_{i,j}^{t,m}$  is evaluated as

$$\mathbb{X}_{i,j}^{t,m} = \mathbb{X}_g \cap \bigcup_{\mathbf{x} \in \mathbf{p}_g(\mathbb{P}_{i,j}^t)} \mathbf{p}_g(\mathbb{C}^t(\mathbf{x})), \quad (38)$$

$$= \mathbb{X}_g \cap (\mathbf{p}_g(\mathbb{P}_{i,j}^t) \oplus \mathbf{p}_g(\mathbb{C}^t(\mathbf{0}))), \quad (39)$$

which, compared to (37), only involves the Minkovski sum of the disc  $\mathbf{p}_g(\mathbb{C}^t(\mathbf{0}))$  and the projection of  $\mathbb{P}_{i,j}^t$  on  $\mathbb{X}_g$ , see Figure 9.

### B. Estimation of the space free of target

In what follows, one shows how UAV  $i$  is able to characterize from  $\mathbf{L}_i$  and  $\mathbf{D}_i$  a subset of  $\mathbb{X}_g$  which contains no target location. For that purpose, the processing of pixels labeled as Ground and as Obstacles is described respectively in Sections IV-B1 and IV-B2.

1) *Using pixels labeled as Ground:* Consider the intersection of the FoV with the ground  $\mathbb{F}(\mathbf{x}_i^u) \cap \mathbb{X}_g$  and a pixel  $(n_r, n_c)$ . The set

$$\mathbb{P}_i^g((n_r, n_c)) = \{\mathbf{x} \in \mathbb{F}(\mathbf{x}_i^u) \cap \mathbb{X}_g \mid \mathbf{p}_c(\mathbf{x}_i^u, \mathbf{x}) \in (n_r, n_c)\} \quad (40)$$

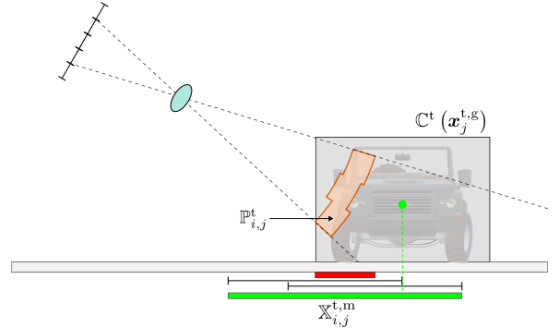


Fig. 9. Estimation of the location of target  $j$ : The set  $\mathbb{P}_{i,j}^t$  is projected on the ground (red set). Then  $\mathbf{p}_g(\mathbb{C}^t)$  (black lines) is used to build  $\mathbb{X}_{i,j}^{t,m}$  (green set). The green dot represents  $\mathbf{x}_j^{t,g}$ .

contains all points in  $\mathbb{F}(\mathbf{x}_i^u) \cap \mathbb{X}_g$  which projection on the CCD array belongs to a pixel classified as ground. According to (28), pixels in  $\mathcal{Y}_i^g$ , i.e., labeled as Ground, are such that only points in  $\mathbb{X}_g$  have contributed to their illumination. Consequently, the set

$$\mathbb{P}_i^g(\mathcal{Y}_i^g) = \{\mathbf{x} \in \mathbb{F}(\mathbf{x}_i^u) \cap \mathbb{X}_g \mid \mathbf{p}_c(\mathbf{x}_i^u, \mathbf{x}) \in \mathcal{Y}_i^g\} \quad (41)$$

of points of  $\mathbb{X}_g$  which projection onto the CCD array belongs to a pixel classified as ground cannot contain the location of a target, see Proposition 6.

*Proposition 6:* For all  $j \in \mathcal{N}^t$ ,  $\mathbf{x}_j^{t,g} \notin \mathbb{P}_i^g(\mathcal{Y}_i^g)$ .

*Proof 7:* First, if  $\mathbf{x}_j^{t,g} \notin \mathbb{F}(\mathbf{x}_i^u)$ , then  $\mathbf{x}_j^{t,g} \notin \mathbb{P}_i^g(\mathcal{Y}_i^g)$ , by definition of  $\mathbb{P}_i^g(\mathcal{Y}_i^g)$ . Consider now  $\mathbf{x}_j^{t,g} \in \mathbb{F}(\mathbf{x}_i^u)$ . According to Section III-C, there exists  $(n_r, n_c) \in \mathcal{N}^t$  such that  $\mathbf{p}_c(\mathbf{x}_i^u, \mathbf{x}_j^{t,g}) \in (n_r, n_c)$ . Moreover, according to Assumption 33, there exists an half-open segment  $[\mathbf{x}_i^c, \mathbf{x}_j^{t,g}[$  such that  $[\mathbf{x}_i^c, \mathbf{x}_j^{t,g}[ \cap \mathbb{S}_j^t(\mathbf{x}_j^t) \neq \emptyset$  while  $[\mathbf{x}_i^c, \mathbf{x}_j^{t,g}[ \cap \mathbb{X}_g = \emptyset$ . Consider the unit vector  $\mathbf{v} \in \mathcal{V}_i(n_r, n_c)$  such that  $\mathbf{v}$  is colinear with  $[\mathbf{x}_i^c, \mathbf{x}_j^{t,g}[$ . Therefore,  $\rho(\mathbf{x}_i^u, \mathbf{v}) \neq d_{\mathbf{v}}(\mathbf{x}_i^c, \mathbb{X}_g)$  and, according to (28),  $\mathbf{p}_c(\mathbf{x}_i^u, \mathbf{x}_j^{t,g}) \notin \mathcal{Y}_i^g$ . Consequently, from (41),  $\mathbf{x}_j^{t,g} \notin \mathbb{P}_i^g(\mathcal{Y}_i^g)$ .

2) *Using pixels labeled as Obstacle:* According to Assumption 8, the distance between a target and any obstacle is at least  $r_s$ . Using pixels labeled as Obstacle, UAV  $i$  is able to characterize an inner-approximation  $\mathbb{X}_g^o \subset \mathbb{X}_g$  of the  $r_s$ -neighborhood of  $\bigcup_{m \in \mathcal{N}^o} \mathbf{p}_g(\mathbb{S}_m^o)$ , the union of the projection on the ground of the shape of all obstacles. Then according to Assumption 8, the set  $\mathbb{X}_g^o$  does not contain any target location.

For pixels labeled as Obstacle, Proposition 8 provides a subset of  $\mathbb{X}_g^o$  intersecting some obstacle  $\mathbb{S}_m^o$ .

*Proposition 8:* If  $(n_r, n_c) \in \mathcal{Y}_i^o$ , then there exists  $m \in \mathcal{N}^o$  such that  $\mathbb{P}_i((n_r, n_c)) \cap \mathbb{S}_m^o \neq \emptyset$ .

*Proof 9:* If  $(n_r, n_c) \in \mathcal{Y}_i^o$ , then, according to (30), for all  $\mathbf{v} \in \mathcal{V}_i(n_r, n_c)$ , there exists  $m \in \mathcal{N}^o$  such that  $\rho(\mathbf{x}_i^u, \mathbf{v}) = d_{\mathbf{v}}(\mathbf{x}_i^c, \mathbb{S}_m^o)$ . Therefore, there exists  $\mathbf{v} \in \mathcal{V}_i(n_r, n_c)$  and there exists  $\mathbf{x} \in \mathbb{S}_m^o$  such that  $d_{\mathbf{v}}(\mathbf{x}_i^c, \{\mathbf{x}\}) = \mathbf{D}_i^0(n_r, n_c)$ . Consequently, from (35),  $\mathbf{x} \in \mathbb{P}_i((n_r, n_c))$ . So there exists  $m \in \mathcal{N}^o$  such that  $\mathbb{P}_i((n_r, n_c)) \cap \mathbb{S}_m^o \neq \emptyset$ .

If  $\mathbf{x} \in \mathbb{P}_i((n_r, n_c)) \cap \mathbb{S}_m^o$  would be known, then, according to (8), one would be able to prove that there cannot be any target in  $\mathbf{p}_g(\mathbb{N}(\{\mathbf{x}\}, r_s))$ . As  $\mathbb{P}_i((n_r, n_c)) \cap \mathbb{S}_m^o$  is only known to be



included in  $\mathbb{P}_i((n_r, n_c))$ , one considers the projection on  $\mathbb{X}_g$  of the set

$$\mathbb{S}^o((n_r, n_c), r_s) = \bigcap_{\mathbf{x} \in \mathbb{P}_i((n_r, n_c))} \mathbb{N}(\{\mathbf{x}\}, r_s). \quad (42)$$

defined as the intersections of the balls  $\mathbb{N}(\{\mathbf{x}\}, r_s)$  for all  $\mathbf{x} \in \mathbb{P}_i((n_r, n_c))$ .  $\mathbb{S}^o((n_r, n_c), r_s)$  is then an estimate of the part of  $\mathbb{X}_0$  that cannot contain a target obtained from  $(n_r, n_c) \in \mathcal{Y}_i^o$ . Then, one gets the following result.

*Proposition 10:* If  $(n_r, n_c) \in \mathcal{Y}_i^o$ , then there exists  $m \in \mathcal{N}^o$ , such that

$$\mathbb{S}^o((n_r, n_c), r_s) \subset \mathbb{N}(\mathbb{S}_m^o, r_s). \quad (43)$$

*Proof 11:* If  $(n_r, n_c) \in \mathcal{Y}_i^o$ , then, according to Proposition 8, there exists  $m \in \mathcal{N}^o$  such that  $\mathbb{P}_i((n_r, n_c)) \cap \mathbb{S}_m^o \neq \emptyset$ . Since  $(\mathbb{P}_i((n_r, n_c)) \cap \mathbb{S}_m^o) \subset \mathbb{S}_m^o$ , one has

$$\mathbb{N}(\mathbb{P}_i((n_r, n_c)) \cap \mathbb{S}_m^o, r_s) \subset \mathbb{N}(\mathbb{S}_m^o, r_s). \quad (44)$$

Then

$$\bigcap_{\mathbf{x} \in \mathbb{P}_i((n_r, n_c))} \mathbb{N}(\{\mathbf{x}\}, r_s) \subset \bigcap_{\mathbf{x} \in \mathbb{P}_i((n_r, n_c)) \cap \mathbb{S}_m^o} \mathbb{N}(\{\mathbf{x}\}, r_s) \quad (45)$$

and  $\mathbb{S}^o((n_r, n_c), r_s) \subset \mathbb{N}(\mathbb{S}_m^o, r_s)$ .

Consequently, an inner-approximation of the  $r_s$ -neighborhood of all the obstacles located within the UAV  $i$  FoV can be obtained by characterizing the union of all  $\mathbb{S}^o((n_r, n_c), r_s)$  over all pixels  $(n_r, n_c) \in \mathcal{Y}_i^o$ . Therefore, UAV  $i$  is able to characterize a set estimate  $\underline{\mathbb{X}}_i^o$  which cannot contain any target location.

*Proposition 12:* If  $\mathcal{Y}_i^o \neq \emptyset$ , then the set defined as

$$\underline{\mathbb{X}}_i^o = \bigcup_{(n_r, n_c) \in \mathcal{Y}_i^o} \mathbf{p}_g(\mathbb{S}^o((n_r, n_c), r_s)) \quad (46)$$

is such that  $\mathbf{x}_j^{t_g} \notin \underline{\mathbb{X}}_i^o$ , for all  $j \in \mathcal{N}^t$ .

*Proof 13:* Using Proposition 10, for each  $(n_r, n_c) \in \mathcal{Y}_i^o$ , there exists  $m \in \mathcal{N}^o$  such that  $\mathbb{S}^o((n_r, n_c), r_s) \subset \mathbb{N}(\mathbb{S}_m^o, r_s)$ . Consequently,

$$\bigcup_{(n_r, n_c) \in \mathcal{Y}_i^o} \mathbb{S}^o((n_r, n_c), r_s) \subset \bigcup_{m \in \mathcal{N}^o} \mathbb{N}(\mathbb{S}_m^o, r_s), \quad (47)$$

which leads to

$$\bigcup_{(n_r, n_c) \in \mathcal{Y}_i^o} \mathbf{p}_g(\mathbb{S}^o((n_r, n_c), r_s)) \subset \bigcup_{m \in \mathcal{N}^o} \mathbf{p}_g(\mathbb{N}(\mathbb{S}_m^o, r_s)). \quad (48)$$

Consequently  $\underline{\mathbb{X}}_i^o \subset \bigcup_{m \in \mathcal{N}^o} \mathbf{p}_g(\mathbb{N}(\mathbb{S}_m^o, r_s))$ . According to Assumption (8), we have

$$\forall j \in \mathcal{N}^t, \mathbf{p}_g(\mathbb{S}_j^t(\mathbf{x}_j^t)) \cap \bigcup_{m \in \mathcal{N}^o} \mathbf{p}_g(\mathbb{N}(\mathbb{S}_m^o, r_s)) = \emptyset, \quad (49)$$

therefore

$$\forall j \in \mathcal{N}^t, \mathbf{p}_g(\mathbb{S}_j^t(\mathbf{x}_j^t)) \cap \underline{\mathbb{X}}_i^o = \emptyset. \quad (50)$$

Moreover, according to (3),  $\mathbf{x}_j^t \in \mathbb{S}_j^t(\mathbf{x}_j^t)$ , then

$$\forall j \in \mathcal{N}^t, \mathbf{x}_j^{t_g} = \mathbf{p}_g(\mathbf{x}_j^t) \notin \underline{\mathbb{X}}_i^o. \quad (51)$$

## C. Estimation of the hidden area

A part of  $\mathbb{F}(\mathbf{x}_i^u) \cap \mathbb{X}_g$  cannot be seen by UAV  $i$  because it has been hidden by an obstacle, a target or an unknown object, and, thus, cannot be labeled as Ground in the image. The pixels labeled either as Obstacle, Target, or Unknown are used to characterize this unseen portion of  $\mathbb{F}(\mathbf{x}_i^u) \cap \mathbb{X}_g$ . This is achieved by evaluating the hidden area  $\mathbb{P}_i^g(\mathcal{Y}_i^o \cup \mathcal{Y}_i^t \cup \mathcal{Y}_i^n)$  which is defined as

$$\mathbb{P}_i^g(\mathcal{Y}_i^o \cup \mathcal{Y}_i^t \cup \mathcal{Y}_i^n) = \bigcup_{(n_r, n_c) \in \mathcal{Y}_i^o \cup \mathcal{Y}_i^t \cup \mathcal{Y}_i^n} \mathbb{P}_i^g((n_r, n_c)) \quad (52)$$

## V. ESTIMATION ALGORITHM

This section describes the way a distributed set-membership target location estimator exploits the information provided by the CVS. It is adapted from [18]. Only the parts related to the exploitation of the CVS are detailed here. The set estimates are initialized at time  $t_0$  as  $\mathcal{L}_{i,0}^t = \emptyset$ ,  $\mathcal{X}_{i,0}^t = \emptyset$ ,  $\bar{\mathbb{X}}_{i,0}^t = \mathbb{X}_g$ , and  $\mathbb{X}_{i,0}^o = \emptyset$ .

### A. Prediction step

At time  $t_k$ , the predicted set  $\bar{\mathbb{X}}_{i,j,k|k-1}^t$  of possible future locations of identified target  $j \in \mathcal{L}_{i,k}^t$  is calculated using the previous locations  $\bar{\mathbb{X}}_{i,j,k-1}^t$ , the target dynamics (2), and the known bounds of its control input:

$$\bar{\mathbb{X}}_{i,j,k|k-1}^t = \mathbf{f}^t(\bar{\mathbb{X}}_{i,j,k-1}^t, [\mathbf{v}^t]) \cap \mathbb{X}_g. \quad (53)$$

In the same way, the predicted set  $\bar{\mathbb{X}}_{i,k|k-1}^t$  for all possible locations of targets still to be identified is

$$\bar{\mathbb{X}}_{i,k|k-1}^t = \mathbf{f}^t(\bar{\mathbb{X}}_{i,k-1}^t, [\mathbf{v}^t]) \cap \mathbb{X}_g. \quad (54)$$

Obstacles being statics, the predicted set  $\mathbb{X}_{i,k|k-1}^o$  is

$$\mathbb{X}_{i,k|k-1}^o = \mathbb{X}_{i,k-1}^o. \quad (55)$$

### B. Measurement update

The CVS of UAV  $i$  provides  $\mathcal{D}_{i,k}^t$ ,  $\bar{\mathbb{X}}_{i,j,k}^{t,m}$ ,  $\mathbb{P}_{i,k}^g(\mathcal{Y}_{i,k}^g)$  and  $\mathbb{P}_{i,k}^g(\mathcal{Y}_{i,k}^g)$ .

Based on Section IV-B2, the  $r_s$ -neighborhoods of all obstacles is updated as  $\mathbb{X}_{i,k|k}^o = \mathbb{X}_{i,k-1}^o \cup \underline{\mathbb{X}}_{i,k}^o$ .

From Sections IV-B1 and IV-B2, the set  $\mathbb{P}_{i,k}^g(\mathcal{Y}_{i,k}^g) \cup \mathbb{X}_{i,k|k}^o$  is proved to be free of target. Thus, the set  $\bar{\mathbb{X}}_{i,k|k-1}^t$  is updated as

$$\bar{\mathbb{X}}_{i,k|k}^t = \bar{\mathbb{X}}_{i,k|k-1}^t \setminus \left( \mathbb{P}_{i,k}^g(\mathcal{Y}_{i,k}^g) \cup \mathbb{X}_{i,k|k}^o \right), \quad (56)$$

Then, regarding the target set estimates, we proved in sections IV-B1 and IV-B2 that  $\mathbb{P}_{i,k}^g(\mathcal{Y}_{i,k}^g) \cup \mathbb{X}_{i,k|k}^o$  cannot contain any target. Therefore, for each previously identified target  $j \in \mathcal{L}_{i,k-1}^t \setminus \mathcal{D}_{i,k}^t$  which is not identified at time  $t_k$ , the update is

$$\bar{\mathbb{X}}_{i,j,k|k}^t = \bar{\mathbb{X}}_{i,j,k|k-1}^t \setminus \left( \mathbb{P}_{i,k}^g(\mathcal{Y}_{i,k}^g) \cup \mathbb{X}_{i,k|k}^o \right). \quad (57)$$

If target  $j$  is identified at time  $t_k$ , i.e.,  $j \in \mathcal{D}_{i,k}^t$ , then according to Section IV-A,  $\mathbf{x}_{j,k}^{\text{t,g}} \in \mathbb{X}_{i,j,k}^{\text{t,m}}$ . Moreover, one has  $\mathbf{x}_{j,k}^{\text{t,g}} \in \mathbb{X}_{i,j,k|k-1}^{\text{t,g}}$  if  $j \in \mathcal{L}_{i,k-1}^t$  or  $\mathbf{x}_{j,k}^{\text{t,g}} \in \overline{\mathbb{X}}_{i,k|k-1}^{\text{t,g}}$  otherwise. Therefore, for each target  $j \in \mathcal{D}_{i,k}^t$ , one has

$$\mathbb{X}_{i,j,k|k}^{\text{t,g}} = \left( \widetilde{\mathbb{X}}_{i,j,k|k-1}^{\text{t,g}} \cap \mathbb{X}_{i,j,k}^{\text{t,m}} \right) \setminus \left( \mathbb{P}_{i,k}^{\text{g}} \left( \mathcal{Y}_{i,k}^{\text{g}} \right) \cup \mathbb{X}_{i,k|k}^{\text{o}} \right), \quad (58)$$

with

$$\widetilde{\mathbb{X}}_{i,j,k|k-1}^{\text{t,g}} = \begin{cases} \mathbb{X}_{i,j,k|k-1}^{\text{t,g}} & \text{if } j \in \mathcal{L}_{i,k-1}^t, \\ \overline{\mathbb{X}}_{i,k|k-1}^{\text{t,g}} & \text{otherwise.} \end{cases} \quad (59)$$

Finally, the list of identified targets becomes  $\mathcal{L}_{i,k|k}^t = \mathcal{L}_{i,k-1}^t \cup \mathcal{D}_{i,k}^t$ .

### C. Update after communication with neighbors

Accounting for the information broadcast by its neighbors, UAV  $i$  updates the list of identified targets  $\mathcal{L}_{i,k}^t = \bigcup_{\ell \in \mathcal{N}_{i,k}} \mathcal{L}_{\ell,k|k}^t$  as well as the  $r_s$ -neighborhoods of all obstacles  $\mathbb{X}_{i,k}^{\text{o}} = \bigcup_{\ell \in \mathcal{N}_{i,k}} \mathbb{X}_{\ell,k|k}^{\text{o}}$  and the set of possible locations of targets still to be detected  $\overline{\mathbb{X}}_{i,k}^{\text{t}} = \bigcap_{\ell \in \mathcal{N}_{i,k}} \overline{\mathbb{X}}_{\ell,k|k}^{\text{t}}$ . Then, if  $j \in \mathcal{L}_{i,k}^t$ , one has  $\mathbb{X}_{i,j,k}^{\text{t,g}} = \bigcap_{\ell \in \mathcal{N}_{i,k}} \widetilde{\mathbb{X}}_{\ell,j,k|k}^{\text{t,g}}$ , with

$$\widetilde{\mathbb{X}}_{i,j,k|k}^{\text{t,g}} = \begin{cases} \mathbb{X}_{i,j,k|k}^{\text{t,g}} & \text{if } j \in \mathcal{L}_{i,k}^t, \\ \overline{\mathbb{X}}_{i,k|k}^{\text{t,g}} & \text{otherwise.} \end{cases} \quad (60)$$

## VI. UAV GUIDANCE LAW DESIGN

The distributed guidance law must be designed so that the trajectories for all UAVs result in reduced uncertainties on the estimated location of both identified and potentially undetected targets. For that purpose, a distributed MPC design [7] based on the one presented in [18] is used to search for the sequence of control inputs  $\mathbf{u}_{i,k:h}^{\text{MPC}} = \left( \mathbf{u}_{i,k}^{\text{MPC}}, \dots, \mathbf{u}_{i,k+h-1}^{\text{MPC}} \right)$  which minimizes the criterion

$$J \left( \mathbf{u}_{i,k:h}^{\text{MPC}} \right) = \Phi_{i,k+h|k}^{\text{x}} + \lambda \Phi_{i,k+h|k}^{\text{d}}, \quad (61)$$

where  $h$  is the prediction horizon,  $\mathbf{u}_{i,\ell}^{\text{MPC}} \in \mathbb{U}^{\text{MPC}}$  is the control input at time  $t_\ell$ , and  $\mathbb{U}^{\text{MPC}}$  is a set of feasible controls.

The cost functions  $\Phi_{i,k+h|k}^{\text{x}}$  and  $\Phi_{i,k+h|k}^{\text{d}}$  are already introduced in [18].  $\Phi_{i,k+h|k}^{\text{x}}$  is a cost related to the predicted reduction of uncertainty described in (34). Its expression is

$$\Phi_{i,k+h|k}^{\text{x}} = \phi \left( \widehat{\mathbb{X}}_{i,k+h}^{\text{t,P}} \right), \quad (62)$$

where  $\widehat{\mathbb{X}}_{i,k+h}^{\text{t,P}} = \overline{\mathbb{X}}_{i,k+h}^{\text{t,P}} \cup \bigcup_{j \in \mathcal{L}_{i,k}^t} \mathbb{X}_{i,j,k+h}^{\text{t,P}}$ , and  $\mathbb{X}_{i,j,k+h}^{\text{t,P}}$  and  $\overline{\mathbb{X}}_{i,k+h}^{\text{t,P}}$  are the prediction sets of the set estimates  $\mathbb{X}_{i,j,k}^{\text{t,g}}$ , for  $j \in \mathcal{L}_{i,k}^t$ , and  $\overline{\mathbb{X}}_{i,k}^{\text{t,g}}$  up to time  $t_{k+h}$ , given the predicted state of UAV  $i$  obtained for the sequence  $\mathbf{u}_{i,k:h}^{\text{MPC}}$ .  $\Phi_{i,k+h|k}^{\text{d}}$  is a cost related to the distance separating UAV  $i$  to the closest predicted set estimate if  $\Phi_{i,k+h|k}^{\text{x}}$  remains constant for any sequence of control inputs. Its expression is

$$\Phi_{i,k+h|k}^{\text{d}} = d \left( \mathbf{p}_g \left( \mathbf{x}_{i,k+h}^{\text{u,P}} \right), \widehat{\mathbb{X}}_{i,k+h}^{\text{t,P}} \setminus \mathbb{P}_{i,k}^{\text{g}} \left( \mathcal{Y}_{i,k}^{\text{o}} \cup \mathcal{Y}_{i,k}^{\text{t}} \cup \mathcal{Y}_{i,k}^{\text{n}} \right) \right). \quad (63)$$

The removal of  $\mathbb{P}_{i,k}^{\text{g}} \left( \mathcal{Y}_{i,k}^{\text{o}} \cup \mathcal{Y}_{i,k}^{\text{t}} \cup \mathcal{Y}_{i,k}^{\text{n}} \right)$  from the predicted sets is due to the fact that as UAV  $i$  couldn't observe this region at time  $t_k$ , and we assume that it won't be able to further observe it whatever the control sequence.

### A. Prediction of set estimates using only UAV own information

The prediction of  $\mathbf{x}_{i,k+\tau}^{\text{u,P}}$  of UAV  $i$  at the prediction step  $\tau \in \{0, \dots, h-1\}$  is performed using a simplified dynamic model  $\mathbf{f}^{\text{u,P}} \left( \mathbf{x}_{i,k+\tau}^{\text{u,P}}, \mathbf{u}_{i,k+\tau}^{\text{MPC}} \right)$  with constant altitude, speed  $v^{\text{u}}$ , and roll and pitch angles set to zeros. The control  $\mathbf{u}_{i,k+\tau}^{\text{MPC}}$  is a yaw angle increment. Using its predicted state  $\mathbf{x}_{i,k+\tau}^{\text{u,P}}$ , UAV  $i$  predicts the resulting FoV  $\mathbb{F} \left( \mathbf{x}_{i,k+\tau}^{\text{u,P}} \right)$ , thus enabling the prediction of the sets  $\overline{\mathbb{X}}_{i,k+\tau+1}^{\text{t,P}}$  and  $\mathbb{X}_{i,j,k+\tau+1}^{\text{t,P}}$ , with  $j \in \mathcal{L}_{i,k}^t$ , similarly to that presented in Section V. The main difference is that only the predicted projection of the FoV can be removed during the correction phase, as the locations of potential obstacles and targets can't be predicted. The correction step for prediction is then:

- prediction of the FoV:

$$\mathbb{F}_{i,k+\tau+1} = \mathbb{F} \left( \mathbf{x}_{i,k+\tau+1}^{\text{u,P}} \right) \setminus \mathbb{P}_{i,k}^{\text{g}} \left( \mathcal{Y}_{i,k}^{\text{o}} \cup \mathcal{Y}_{i,k}^{\text{t}} \cup \mathcal{Y}_{i,k}^{\text{n}} \right) \quad (64)$$

- correction of the predicted sets:

$$\mathbb{X}_{i,j,k+\tau+1}^{\text{t,P}} = \mathbb{X}_{i,j,k+\tau+1|k+\tau}^{\text{t,P}} \setminus \mathbb{F}_{i,k+\tau+1}, j \in \mathcal{L}_{i,k}^t \quad (65)$$

$$\overline{\mathbb{X}}_{i,k+\tau+1}^{\text{t,P}} = \overline{\mathbb{X}}_{i,k+\tau+1|k+\tau}^{\text{t,P}} \setminus \mathbb{F}_{i,k+\tau+1}. \quad (66)$$

### B. Cooperative design

If there exists other UAVs in the neighborhood of UAV  $i$ , it is of interest to account for their predicted trajectories for evaluating the predicted sets. Let  $\mathbb{F}_{\ell,k+\tau+1}$  be the predicted FoV for  $\ell \in \mathcal{N}_{i,k}$ , using information broadcast of  $\mathbb{P}_{\ell,k}^{\text{g}} \left( \mathcal{Y}_{\ell,k}^{\text{o}} \cup \mathcal{Y}_{\ell,k}^{\text{t}} \cup \mathcal{Y}_{\ell,k}^{\text{n}} \right)$  UAV  $i$  is able to evaluate the set

$$\mathbb{F}_{i,k+\tau+1}^{\mathcal{N}} = \bigcup_{\ell \in \mathcal{N}_{i,k}} \mathbb{F}_{\ell,k+\tau+1} \quad (67)$$

representing the predicted zone of the RoI that would be observed by the sub-fleet  $\mathcal{N}_{i,k}$ . Consequently, the corrections (65) and (66) become

$$\mathbb{X}_{i,j,k+\tau+1}^{\text{t,P}} = \mathbb{X}_{i,j,k+\tau+1|k+\tau}^{\text{t,P}} \setminus \mathbb{F}_{i,k+\tau+1}^{\mathcal{N}}, j \in \mathcal{L}_{i,k}^t \quad (68)$$

$$\overline{\mathbb{X}}_{i,k+\tau+1}^{\text{t,P}} = \overline{\mathbb{X}}_{i,k+\tau+1|k+\tau}^{\text{t,P}} \setminus \mathbb{F}_{i,k+\tau+1}^{\mathcal{N}}. \quad (69)$$

## VII. SIMULATIONS

The simulations have been performed using Webots<sup>1</sup> environment to generate the measurement collected by the UAVs, while the algorithms are implemented on MATLAB.

### A. Simulation conditions

The RoI is  $\mathbb{X}_0 = [-250 \text{ m}, 250 \text{ m}] \times [-250 \text{ m}, 250 \text{ m}] \times \mathbb{R}^+$  which contains  $N^{\text{t}} = 8$  targets (8 cars in the proposed simulation). The RoI corresponds to a simplified urban environment scattered with different kind of buildings. Figure 10 shows the map considered for the simulation. The area covered by the chosen obstacles corresponds to 5 % of the area of the ground  $\mathbb{X}_g$ . The height of all obstacles is lower than 50 m.

<sup>1</sup><https://cyberbotics.com/doc/guide/index>

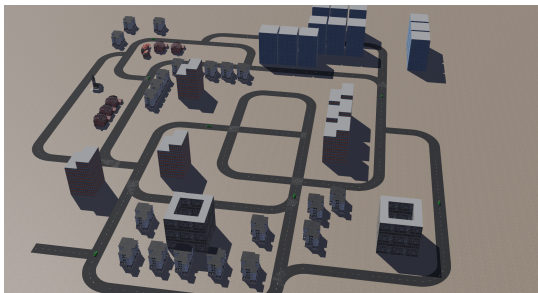


Fig. 10. Simulated urban environment in Webots

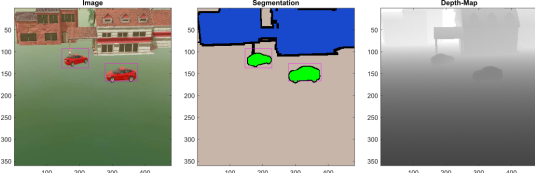


Fig. 11. Illustration of the CVS information provided to MatLab by the sensors simulated by Webots

The dimension of each car is  $4.6 \text{ m} \times 1.8 \text{ m} \times 1.5 \text{ m}$ , which correspond to a cylinder  $\mathbb{C}^t$  of radius  $r^t = 2.5 \text{ m}$ , and height  $h^t = 2 \text{ m}$ . A safety distance  $r_s$  between targets and obstacles of  $3 \text{ m}$  is assumed. The state  $\mathbf{x}_{j,k}^t = (x_{j,1,k}^t, x_{j,2,k}^t, x_{j,3,k}^t)$  of target  $j \in \mathcal{N}^t$  consists of the coordinates  $(x_{j,1,k}^t, x_{j,2,k}^t)$  of the projection on  $\mathbb{X}_g$  of its center of mass, and of its heading angle  $x_{j,3,k}^t$ . Its dynamic (2) is

$$\begin{pmatrix} x_{j,1,k+1}^t \\ x_{j,2,k+1}^t \\ x_{j,3,k+1}^t \end{pmatrix} = \begin{pmatrix} x_{j,1,k}^t + T v_{j,1,k}^t \cos(x_{j,3,k}^t) \\ x_{j,2,k}^t + T v_{j,1,k}^t \sin(x_{j,3,k}^t) \\ x_{j,3,k}^t + T v_{j,2,k}^t \end{pmatrix}, \quad (70)$$

where  $v_{j,1,k}^t$  is the target speed and  $v_{j,2,k}^t$  is the target turn rate. During the simulation,  $v_{j,1,k}^t$  is randomly chosen in a given interval at each time step. Moreover,  $v_{j,2,k}^t$  is chosen such as the car stays on the road. Note that the UAVs do not exploit any knowledge related to the roads during the search exploration.

A fleet of 4 identical quadcopters is considered (the model DJI Mavic2Pro of Webots has been chosen). These UAVs are assumed to be equipped with a camera of resolution  $N_r \times N_c = 360 \times 480$  pixels, an aperture angle of  $\pi/4$  rad and, an orientation regarding to the UAV body frame of  $\theta = \pi/6$  rad. A depth-map is provided by the *range-finder* of Webots with the same resolution as the camera. Its maximal measurement range is set to  $d_{\max} = 300 \text{ m}$  and the bounds of the noise  $w$  expressed in (25) are set at  $[\underline{w}, \bar{w}] = [-1\%, 1\%]$ . For example, if the measured distance  $\mathbf{D}_i^0$  for a perceived object is  $200 \text{ m}$ , the registered depth  $\mathbf{D}_i$  belongs to the interval  $[198 \text{ m}, 202 \text{ m}]$ . Figure 11 shows the CVS information provided by the sensors embedded on each UAV.

The control input  $\mathbf{u}_{i,k}^{\text{MPC}}$  for the simplified UAV dynamic model introduced in Section VI-A, *i.e.*, the yaw angular increment, is taken in  $\mathbb{U}^{\text{MPC}} = \{-\pi/3, -\pi/6, 0, \pi/6, \pi/3\}$ . Furthermore, the prediction horizon of the MPC is set to  $h =$

2. Then, the MPC provides an input to a low-level controller which consist of a PID controller designed to also ensure a constant speed module of  $5 \text{ m/s}$  and a constant fly-height. In order to avoid collision, this fly-height is different for each UAV, and is higher than any obstacle height. Furthermore, no restriction is considered on the communication range between UAVs.

The CVS refresh-rate is  $T = 0.5 \text{ s}$ , and the estimation algorithm presented in Sections IV and V is done after each new acquisition of CVS information. However, the period with which the MPC updates its guidance law is set at  $3 \text{ s}$  because of the relative slowness of the quadcopter dynamics compared to the CVS refresh-rate. This choice is made in order to ensure that each UAV has enough time to reach the desired yaw angle input designed by the MPC.

For the consistency of the simulations, a trade-off between map size, target speed, UAV speed and computer performances has to be solved. Indeed, the size of the RoI has to be consistent with the target maximal speed in order to guarantee realistic dynamics: the faster the target, the larger the RoI. Moreover, an increase in the target maximal speed induces the necessity of increasing the UAV speed. Then, for higher target maximal speed, and thus larger RoI, more UAVs with higher speed are needed to maintain an efficient exploration of the search area, which increase dramatically the simulation time. Therefore, the faster the targets, the heavier the simulation. To avoid high time-consuming simulations, we set the target maximal speed at  $1 \text{ m/s}$ . Thus, the speed ratio between the UAVs and the targets is equal or above 5. The introduction of traditional car speeds should not change the following simulation results, since it is a scaling problem (faster targets, faster UAVs, larger map. . .).

## B. Results

10 independent simulations have been run during  $300 \text{ s}$ . The numerical and graphical results presented in this subsection are obtained by averaging the 10 simulations' results.

Figure 12 and the video<sup>2</sup> illustrates a typical evolution at 4 different time instants (for the figure) of the set  $\bar{\mathbb{X}}_{i,k}^t$  containing undetected targets (in yellow), the sets  $\bar{\mathbb{X}}_{i,j,k}^t$  gathering all the possible locations of their related identified target (in green), and the set  $\mathbb{X}_{i,k}^o$  representing the inner-approximation of  $r_s$ -neighborhood of the detected obstacles (in black). A new set  $\mathbb{X}_{i,k}^h$  (in blue) is introduced here. It represents the portion of  $\mathbb{X}_g$  that has not been seen by UAV  $i$  at a previous time instant due to an occlusion by an obstacle while not being eliminated until  $t_k$ . Its update is done as

$$\mathbb{X}_{i,k}^h = \left( \mathbb{X}_{i,k-1}^h \cup \mathbb{P}_{i,k}^g (\mathcal{Y}_{i,k}^o \cup \mathcal{Y}_{i,k}^t \cup \mathcal{Y}_{i,k}^n) \right) \setminus \mathbb{P}_{i,k}^g (\mathcal{Y}_{i,k}^g) \quad (71)$$

with  $\mathbb{X}_{i,0}^h = \emptyset$ . Remind that  $\mathbb{P}_i^g (\mathcal{Y}_{i,k}^o \cup \mathcal{Y}_{i,k}^t \cup \mathcal{Y}_{i,k}^n)$  is the occluded portion of  $\mathbb{X}_g$  from UAV  $i$  point of view, and  $\mathbb{P}_{i,k}^g (\mathcal{Y}_{i,k}^g)$  is the portion of  $\mathbb{X}_g$  covered by UAV  $i$  FoV at

<sup>2</sup><https://nextcloud.centralesupelec.fr/s/Sxf5Nk2RJRXYzk>

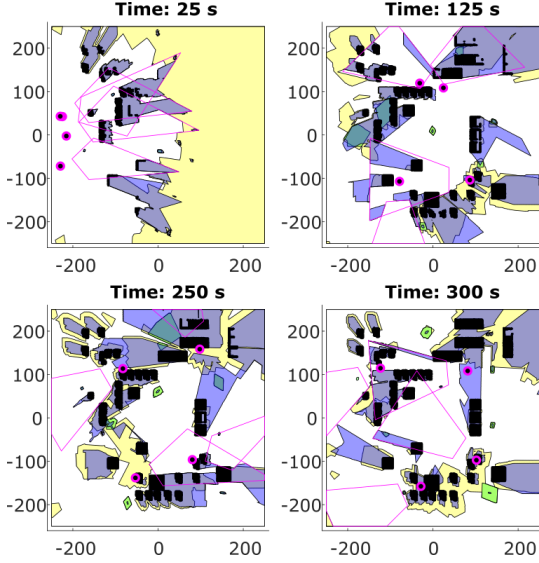


Fig. 12. Evolution of the set estimates  $\mathbb{X}_{i,j,k}^t$  (green),  $\bar{\mathbb{X}}_{i,k}^t$  (yellow),  $\mathbb{X}_{i,k}^o$  (black) and  $\mathbb{X}_{i,k}^h$  (blue) at different time instant; The UAVs and the intersection of their FoV with the ground are represented in purple. Targets are not represented.

Name	Description
Theoretical coverage	$\Phi(\mathbb{F}_k) = \phi\left(\bigcup_{i \in \mathcal{N}^u} (\mathbb{F}(\mathbf{x}_{i,k}^u) \cap \mathbb{X}_g)\right)$
Effective coverage	$\Phi(\mathcal{Y}_k^g) = \phi\left(\bigcup_{i \in \mathcal{N}^u} \mathbb{P}_i^g(\mathcal{Y}_{i,k}^g)\right)$
Area explored	$\Phi(\mathbb{X}_k^g) = \phi\left(\bigcup_{t=1}^k \bigcup_{\ell \in \mathcal{N}_{i,t}} \mathbb{P}_{\ell,t}^g(\mathcal{Y}_{\ell,t}^g)\right)$
Position uncertainty	$\Phi(\mathcal{X}_{i,k}^t) = \frac{\sum_{j \in \mathcal{L}_{i,k}^t} \phi(\bar{\mathbb{X}}_{i,j,k}^t)}{\text{card}(\mathcal{L}_{i,k}^t)}$
Localization error	$e(\mathcal{X}_{i,k}^t) = \frac{\sum_{j \in \mathcal{L}_{i,k}^t} \ \mathbf{x}_{j,k}^{t^g} - c(\bar{\mathbb{X}}_{i,j,k}^t)\ }{\text{card}(\mathcal{L}_{i,k}^t)}$
Unexplored area (UA)	$\phi(\bar{\mathbb{X}}_{i,k}^t)$
Occluded UA	$\phi(\bar{\mathbb{X}}_{i,k}^t \cap \mathbb{X}_{i,k}^h)$

TABLE I

METRICS USED TO ANALYZE THE ALGORITHM'S PERFORMANCES. NOTE THAT MOST METRICS ARE RATHER EXPRESSED AS  $\Phi(\cdot) / \phi(\mathbb{X}_G)$ .

time  $t_k$  that is proved to be the ground. Then, UAV  $i$  accounts for the information broadcast by its neighbors by doing

$$\mathbb{X}_{i,k}^h = \left( \bigcup_{\ell \in \mathcal{N}_{i,k}^h} \mathbb{X}_{\ell,k|k}^h \right) \setminus \left( \bigcup_{\ell \in \mathcal{N}_{i,k}^g} \mathbb{P}_{\ell,k}^g(\mathcal{Y}_{\ell,k}^g) \right). \quad (72)$$

Since there is no restriction on their communication range, all UAVs share the same set estimates. Therefore, the index  $i$  is irrelevant in most cases.

The metrics used to evaluate the performances of the proposed algorithm are defined in Table I.

As shown in Figure 13, the fleet may theoretically monitor 27% of the RoI (average evolution of  $\Phi(\mathbb{F}_k)$  in black dashed line), but, due to the presence of unknown obstacles, the effective map coverage of the fleet (average evolution of  $\Phi(\mathcal{Y}_k^g)$  in green dashed line) decreases to almost 18%. Therefore, one third of the UAV FoV is cluttered by obstacles.

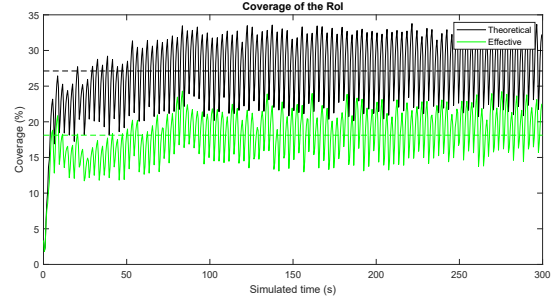


Fig. 13. Mean value over 10 simulations of  $\Phi(\mathbb{F}_k) / \phi(\mathbb{X}_g)$  and  $\Phi(\mathcal{Y}_k^g) / \phi(\mathbb{X}_g)$ . Dashed lines are the temporal mean values.

Note that in order to simulate the entry of the fleet in the RoI, all UAVs start outside the RoI and around the same initial position, *i.e.*, they do not enter the RoI from different directions. Thus, the fleet needs some time to enter the RoI, to spread and start the exploration.

The oscillatory behavior of the curves is explained by the behavior of the low-level controller. Indeed, each time the yaw angle is updated by the MPC (that may occur every 3 s), the pitch angle is also impacted by this change due to the UAV dynamics, before being corrected by the low-level controller designed to maintain a constant speed. Thus, since the camera is fixed in the UAV frame, the UAV FoV is also changing with the same period.

To evaluate the performances of the proposed approach in searching, finding and locating the targets, the evolution of metrics 3 to 7 from Table I are provided in Figure 14.

The area explored  $\Phi(\mathbb{X}_k^g)$  (in purple) evaluates the area of the map proved to be the ground. Since around 5% of  $\mathbb{X}_g$  is occupied by obstacles, the maximum theoretical value of  $\Phi(\mathbb{X}_k^g)$  is 95%. It can be seen, that after 5 minutes,  $\Phi(\mathbb{X}_k^g)$  stagnates at around 93 %, meaning that the fleet has explored nearly all the RoI. The remaining 2 % originate from areas located around buildings at the fringes of the map, which are hard to be observed by the UAVs, because the criterion implemented in the MPC does not motivate them to observe these areas. Indeed, for making such observations, the UAVs would have their FoV outside of the RoI, while turning around the obstacles.

The metric  $\Phi(\mathcal{X}_{i,k}^t)$  (in green), which evaluates the average localization uncertainty for each already identified targets, is stabilized at around 0.25 % of  $\phi(\mathbb{X}_g)$  with a standard deviation of 0.16 %, which represents a surface of a disc with a radius between 8.2 m and 18.2 m. The remaining localization uncertainty comes partly from the absence of knowledge of the target dynamic (apart from their maximal velocity), which does not enable the UAVs to efficiently predict the evolution of the identified targets.

However, as seen in Figure 14 - B, the localization error  $e(\mathcal{X}_{i,k}^t)$  (in red) between the target real location and the barycenter of its set estimate is about  $1.0 \text{ m} \pm 0.4 \text{ m}$ , which stays smaller than the radius  $r^t = 2.5 \text{ m}$  of the cylinder  $\mathbb{C}^t$  representing an outer-approximation of the target shape. Thus, despite knowing only the target maximal speed, the UAV fleet manages to accurately localize the identified targets.

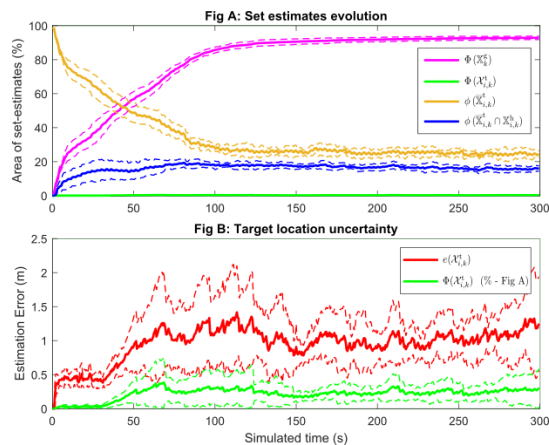


Fig. 14. Top: mean value with standard deviation over 10 simulations of  $\Phi(\mathbb{X}_g^t)/\phi(\mathbb{X}_g)$  (purple),  $\Phi(\mathcal{X}_{i,k}^t)/\phi(\mathbb{X}_g)$  (green; no standard deviation),  $\phi(\overline{\mathbb{X}}_{i,k}^t)/\phi(\mathbb{X}_g)$  (orange),  $\phi(\overline{\mathbb{X}}_{i,k}^t \cap \mathbb{X}_{i,k}^h)/\phi(\mathbb{X}_g)$  (blue). Bottom: mean value with standard deviation of  $\Phi(\mathcal{X}_{i,k}^t)/\phi(\mathbb{X}_g)$  (green) and  $e(\mathcal{X}_{i,k}^t)$  (red).

The set estimate  $\phi(\overline{\mathbb{X}}_{i,k}^t)$  (in orange in Figure 14 - A) containing locations of potential undetected targets decreases to finally stagnate at around  $25.5\% \pm 2.7\%$ , whereas all targets have been found in almost 150 seconds (light blue curve in Figure 15).

According to Figure 14 - A, almost two third of the set  $\phi(\overline{\mathbb{X}}_{i,k}^t)$  remaining at the end of the simulation belongs to  $\phi(\overline{\mathbb{X}}_{i,k}^t \cap \mathbb{X}_{i,k}^h)$  (in blue), and thus corresponds to a portion of  $\overline{\mathbb{X}}_{i,k}^t$  that cannot be eliminated because of the presence of an obstacle, and that continues to grow until observed from another point of view. These results directly illustrate the limit of the criterion 61 to design a guidance law which bypasses the obstacle in order to rapidly and cooperatively monitor the previously occluded regions.

The difference between the number of targets that are within the FoV (in black bar graph in Figure 15) and the number of targets that are currently identified (blue bar graph) shows that it is common for a UAV to be hindered by an obstacle when it tries to recapture a target. This problem of mismanagement of the obstacle volume will be treated in future work.

## VIII. CONCLUSION

This paper presents the first algorithm which exploits CVS information along set-membership hypotheses to solve a CSAT problem in an unknown and cluttered environment. To achieve this goal, we proposed several hypotheses related to the interpretation of the information provided by CVS in order to make it compliant with set-membership techniques. Those hypotheses consist mainly of a model for the depth measurement, and the confidence we have when a pixel is labeled Target or Ground. Then, the proposed algorithm estimates the location of detected and identified targets by characterizing a set estimate which guarantees to contain their true location. Once the estimation is done, each UAV updates its knowledge through a prediction-correction process which

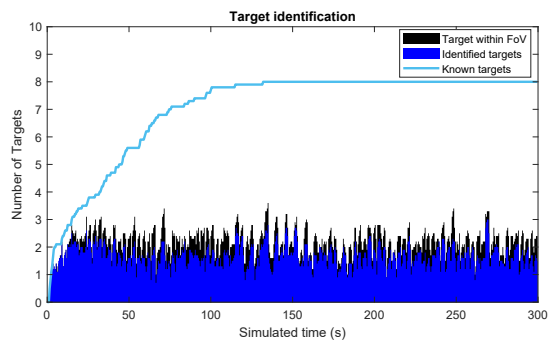


Fig. 15. Mean value over 10 simulations. The light blue curve is the mean of the number of identified targets  $\mathcal{L}_{i,k}^t$ . The black bar graph is the number of targets with  $\mathbf{x}_{j,k}^{t,g}$  within the FoV of at least one UAV. The blue bar graph is the number of identified target at the current time.

accounts for the information broadcast by neighbors. Finally, each UAV designs a new guidance law through a cooperative distributed MPC. Even if the target detection is not perfectly reliable in practice, the classification of a pixel as Unknown, *i.e.*, neither Ground nor Target nor Obstacle, adds a layer of security to avoid removing potential locations for a target that the UAV has failed to detect. The proposed set-membership CSAT algorithm is tested in simulation with a simplified urban environment. The estimation error regarding the location of the identified targets remains small despite the fact that UAVs have only access to an over-approximated target shape. However, even if the RoI has been almost entirely explored at the end of each simulation, the current guidance law does not enable the UAVs to efficiently explore around obstacles in order to eliminate the potential undetected target locations. Consequently, without more UAVs deployed into the RoI, the fleet is has some difficulties to explore the environment in order to eliminate the probability that there still exist undetected targets evolving within the RoI.

This downside of our approach will be addressed in further research directions such as the creation of a 3D map of the RoI in order to predict the portion of the ground that would not be observed during the design of the guidance law. Other research directions may be considered such as the addition of false alarms and none detection of target by the embedded CVS.

## APPENDIX

### A. Proof of Proposition 4

The following corollary is helpful to characterize an estimate of the possible locations of target  $j$  from  $\mathbf{p}_g(\mathbb{P}_{i,j}^t)$ .

*Corollary 14:* If  $j \in \mathcal{D}_i^t$ , then  $\mathbf{p}_g(\mathbb{P}_{i,j}^t) \cap \mathbf{p}_g(\mathbb{S}_j^t(\mathbf{x}_j^t)) \neq \emptyset$ .

*Proof 15:* Consider the sets  $\mathbb{A}$  and  $\mathbb{B}$ . If  $\mathbb{A} \cap \mathbb{B} \neq \emptyset$ , then we have  $\mathbf{p}_g(\mathbb{A} \cap \mathbb{B}) \subset \mathbf{p}_g(\mathbb{A}) \cap \mathbf{p}_g(\mathbb{B})$ . Therefore, if  $j \in \mathcal{D}_i^t$ , then from Corollary 3, we have  $\mathbb{P}_{i,j}^t \cap \mathbb{S}_j^t(\mathbf{x}_j^t) \neq \emptyset$ . Consequently,  $\mathbf{p}_g(\mathbb{P}_{i,j}^t) \cap \mathbf{p}_g(\mathbb{S}_j^t(\mathbf{x}_j^t)) \neq \emptyset$ .

If some  $\mathbf{x} \in \mathbf{p}_g(\mathbb{S}_j^t(\mathbf{x}_j^t))$  is available, then the set  $\mathbf{p}_g(\mathbb{C}^t(\mathbf{x}))$  contains  $\mathbf{x}_j^{t,g}$  and can serve as a set estimate of the target location, as stated by the following proposition.

*Proposition 16:* If  $j \in \mathcal{N}^t$  and  $\mathbf{x} \in \mathbf{p}_g(\mathbb{S}_j^t(\mathbf{x}_j^t))$ , then  $\mathbf{x}_j^{t,g} \in \mathbf{p}_g(\mathbb{C}^t(\mathbf{x}))$ .



*Proof 17:* Consider some  $\mathbf{x} \in \mathbf{p}_g(\mathbb{S}_j^t(\mathbf{x}_j^t))$ . Since  $\mathbb{S}_j^t(\mathbf{x}_j^t) \subset \mathbb{C}^t(\mathbf{x}_j^{t,g})$ ,  $\mathbf{p}_g(\mathbb{S}_j^t(\mathbf{x}_j^t)) \subset \mathbf{p}_g(\mathbb{C}^t(\mathbf{x}_j^{t,g}))$  and  $\mathbf{x} \in \mathbf{p}_g(\mathbb{C}^t(\mathbf{x}_j^{t,g}))$ . As  $\mathbf{p}_g(\mathbb{C}^t(\mathbf{x}_j^{t,g}))$  is the disc of center  $\mathbf{x}_j^{t,g}$  and radius  $r^t$ , one has  $\|\mathbf{x} - \mathbf{x}_j^{t,g}\| \leq r^t$ . The projection  $\mathbf{p}_g(\mathbb{C}^t(\mathbf{x}))$  of the circular right cylinder  $\mathbb{C}^t(\mathbf{x})$  on  $\mathbb{X}_g$  is the disc of center  $\mathbf{x}$  and radius  $r$ . Consequently, as  $\|\mathbf{x} - \mathbf{x}_j^{t,g}\| \leq r^t$ ,  $\mathbf{p}_g(\mathbb{C}^t(\mathbf{x}))$  contains  $\mathbf{x}_j^{t,g}$ .

Now, all ingredients are present for the proof of Proposition 4.

As  $j \in \mathcal{D}_i^t$ , using Corollary 14, one has  $\mathbf{p}_g(\mathbb{P}_{i,j}^t) \cap \mathbf{p}_g(\mathbb{S}_j^t(\mathbf{x}_j^t)) \neq \emptyset$ . So, there exists  $\mathbf{x} \in \mathbf{p}_g(\mathbb{P}_{i,j}^t) \cap \mathbf{p}_g(\mathbb{S}_j^t(\mathbf{x}_j^t)) \subset \mathbf{p}_g(\mathbb{S}_j^t(\mathbf{x}_j^t))$ . Consequently, from Proposition 16, one has  $\mathbf{x}_j^{t,g} \in \mathbf{p}_g(\mathbb{C}^t(\mathbf{x}))$ . As  $\mathbf{p}_g(\mathbb{S}_j^t(\mathbf{x}_j^t))$  and  $\mathcal{Y}_{i,j}^t$  are unknown, to build a set estimate for  $\mathbf{x}_j^{t,g}$ , one has to consider all  $\mathbf{x} \in \mathbf{p}_g(\mathbb{P}_{i,j}^t)$  and build the union of  $\mathbf{p}_g(\mathbb{C}^t(\mathbf{x}))$  over all  $\mathbf{x} \in \mathbf{p}_g(\mathbb{P}_{i,j}^t)$ .

### B. Characterization of $\mathbb{X}_{i,j}^{t,m}$ and $\mathbb{X}_i^o$

This section describes an approach to get an outer-approximation of the set estimate  $\mathbb{X}_{i,j}^{t,m}$  introduced in IV-A as well as an inner-approximation of  $\mathbb{X}_i^o$  introduced in Section IV-B2. The determination of both sets requires the characterization of  $\mathbb{P}_i((n_r, n_c))$  defined in (35). Consider a pixel  $(n_r, n_c)$ . The set  $\mathbb{P}_i((n_r, n_c))$  is the intersection between the half cone of apex  $\mathbf{x}_i^c$  and vertices corresponding to one of the four unit vectors  $\mathbf{M}_{\mathcal{F}_i^c}^{\mathcal{F}_i^c} \mathbf{v}_\ell^{\mathcal{F}_i^c}$ ,  $\ell = 1, \dots, 4$  with  $\mathbf{v}_1^{\mathcal{F}_i^c} = \mathbf{v}^{\mathcal{F}_i^c}(n_c, n_r)$ ,  $\mathbf{v}_2^{\mathcal{F}_i^c} = \mathbf{v}^{\mathcal{F}_i^c}(n_c, n_r - 1)$ ,  $\mathbf{v}_3^{\mathcal{F}_i^c} = \mathbf{v}^{\mathcal{F}_i^c}(n_c - 1, n_r - 1)$ , and  $\mathbf{v}_4^{\mathcal{F}_i^c} = \mathbf{v}^{\mathcal{F}_i^c}(n_c, n_r - 1)$  and the space between the two spheres of center  $\mathbf{x}_i^c$  and radii  $\frac{1}{1+w} \mathbf{D}_i(n_r, n_c)$  and  $\frac{1}{1+w} \mathbf{D}_i(n_r, n_c)$ . See figure 4 where the 4 vectors  $\mathbf{v}_\ell^{\mathcal{F}_i^c}$  are represented by the blue lines. A truncated pyramidal outer-approximation  $\overline{\mathbb{P}}_i((n_r, n_c))$  of  $\mathbb{P}_i((n_r, n_c))$  is easily built. For that purpose, consider the angle  $\theta_\ell$  between the  $\mathbf{v}_\ell^{\mathcal{F}_i^c}$  with  $\mathbf{v}^{\mathcal{F}_i^c}(n_c - 0.5, n_r - 0.5)$ , the unit vector defining the light-ray illuminating the center of the pixel. The eight vertices defining  $\overline{\mathbb{P}}_i((n_r, n_c))$  are, with  $\ell \in \{1, 2, 3, 4\}$

$$\underline{\mathbf{x}}_\ell^p = \mathbf{x}_i^c + \frac{1}{1+w} \mathbf{D}_i(n_r, n_c) \mathbf{M}_{\mathcal{F}_i^c}^{\mathcal{F}_i^c} \mathbf{v}_\ell^{\mathcal{F}_i^c}, \quad (73)$$

$$\overline{\mathbf{x}}_\ell^p = \mathbf{x}_i^c + \frac{1}{\cos(\theta_\ell) (1+w)} \mathbf{D}_i(n_r, n_c) \mathbf{M}_{\mathcal{F}_i^c}^{\mathcal{F}_i^c} \mathbf{v}_\ell^{\mathcal{F}_i^c}. \quad (74)$$

Then, the evaluation of  $\mathbb{X}_{i,j}^{t,m}$  requires the determination of the projection  $\mathbf{p}_g(\mathbb{P}_{i,j}^t)$ , with  $\mathbb{P}_{i,j}^t$  being the union of the sets  $\mathbb{P}_i((n_r, n_c))$ , for all  $(n_r, n_c) \in [\mathcal{Y}_{i,j}^t] \cap \mathcal{Y}_i^t$ .  $\mathbf{p}_g(\mathbb{P}_{i,j}^t)$  is the union of the sets  $\mathbf{p}_g(\mathbb{P}_i((n_r, n_c)))$  over  $(n_r, n_c) \in [\mathcal{Y}_{i,j}^t] \cap \mathcal{Y}_i^t$ . Since  $\mathbb{P}_i((n_r, n_c)) \subset \overline{\mathbb{P}}_i((n_r, n_c))$  and  $\overline{\mathbb{P}}_i((n_r, n_c))$  is a convex set, an outer-approximation of  $\mathbf{p}_g(\mathbb{P}_i((n_r, n_c)))$  is obtained by characterizing the convex hull of  $\mathbf{p}_g(\overline{\mathbb{P}}_i((n_r, n_c)))$ . Finally, an outer-approximation of  $\mathbb{X}_{i,j}^{t,m}$  is obtained as  $\mathbb{X}_g \cap (\mathbf{p}_g(\overline{\mathbb{P}}_{i,j}^t) \oplus \mathbf{p}_g(\mathbb{C}^t(\mathbf{0})))$ , with  $\mathbf{p}_g(\overline{\mathbb{P}}_{i,j}^t)$  being the union of  $\mathbf{p}_g(\overline{\mathbb{P}}_i((n_r, n_c)))$  over  $(n_r, n_c) \in [\mathcal{Y}_{i,j}^t] \cap \mathcal{Y}_i^t$ .

The set  $\mathbb{X}_i^o$  is the union of the projections of the sets  $\mathbb{S}^o((n_r, n_c), r_s)$  on the ground, for all  $(n_r, n_c) \in \mathcal{Y}_i^o$ . These sets So are defined in 42 as the intersection of all spheres

$\mathbb{N}(\{\mathbf{x}\}, r_s)$  with center  $\mathbf{x} \in \mathbb{P}_i((n_r, n_c))$  and radius  $r_s$ . Since  $\mathbb{P}_i((n_r, n_c)) \subset \overline{\mathbb{P}}_i((n_r, n_c))$ , we have

$$\bigcap_{\mathbf{x} \in \overline{\mathbb{P}}_i((n_r, n_c))} \mathbb{N}(\{\mathbf{x}\}, r_s) \subset \bigcap_{\mathbf{x} \in \mathbb{P}_i((n_r, n_c))} \mathbb{N}(\{\mathbf{x}\}, r_s). \quad (75)$$

Then, according to (42), we have

$$\bigcap_{\mathbf{x} \in \overline{\mathbb{P}}_i((n_r, n_c))} \mathbb{N}(\{\mathbf{x}\}, r_s) \subset \mathbb{S}^o((n_r, n_c), r_s). \quad (76)$$

Moreover, as  $\overline{\mathbb{P}}_i((n_r, n_c))$  is convex, we have

$$\bigcap_{\mathbf{x} \in \overline{\mathbb{P}}_i((n_r, n_c))} \mathbb{N}(\{\mathbf{x}\}, r_s) = \bigcap_{\mathbf{x} \in \overline{\mathbb{P}}_i(n_r, n_c)} \mathbb{N}(\{\mathbf{x}\}, r_s), \quad (77)$$

with  $\overline{\mathbb{P}}_i(n_r, n_c) = \{\underline{\mathbf{x}}_1^p, \dots, \underline{\mathbf{x}}_4^p, \overline{\mathbf{x}}_1^p, \dots, \overline{\mathbf{x}}_4^p\}$ . An inner approximation of  $\mathbb{S}^o((n_r, n_c), r_s)$  is then obtained as the intersection of 8 spheres of radius  $r_s$  and centers in the set  $\overline{\mathbb{P}}_i(n_r, n_c)$ . As this intersection is still complex to characterize, an inner approximation of the intersection may be obtained by determining the at most two points belonging to the intersection of all three spheres among the eight [8] and selecting among those points those that belong to the remaining five other spheres. The resulting convex hull  $\mathbb{S}^o((n_r, n_c))$  of all the points that have been obtained is still an inner approximation of  $\mathbb{S}^o((n_r, n_c), r_s)$ . Finally, an inner-approximation of  $\mathbb{X}_i^o$  is obtained by evaluating  $\mathbf{p}_g(\bigcup_{(n_r, n_c) \in \mathcal{Y}_i^o} \mathbb{S}^o((n_r, n_c)))$ .

*Remark 1:* the computation of an outer approximation of  $\mathbb{P}_i((n_r, n_c))$  could also be obtained using interval analysis [20] but would result in larger approximation.

### C. Characterization of $\mathbb{P}_i^g(\mathcal{Y}_i^g)$ and $\mathbb{P}_i^g(\mathcal{Y}_i^o \cup \mathcal{Y}_i^t \cup \mathcal{Y}_i^n)$

To evaluate  $\mathbb{P}_i^g(\mathcal{Y}_i^g)$  introduced in (41), the union of sets  $\mathbb{P}_i^g((n_r, n_c))$  for  $(n_r, n_c) \in \mathcal{Y}_i^g$  has to be characterized. Neglecting the limitation of the FoV by  $\mathbb{B}(\mathbf{x}_i^u, d_{\max})$  and as  $\mathbb{X}_g$  is a part of a plane,  $\mathbb{P}_i^g((n_r, n_c))$  is the convex quadrangle defined by the intersection of  $\mathbb{X}_g$  with the half-cone of apex  $\mathbf{x}_i^c$  and edges related to the four unit vector  $\mathbf{v}_\ell^{\mathcal{F}_i^c}$ , with  $\ell = 1, \dots, 4$ , see Figure 4.  $\mathbb{P}_i^g(\mathcal{Y}_i^g)$  is then the union of the convex quadrangles  $\mathbb{P}_i^g((n_r, n_c))$  for all  $(n_r, n_c) \in \mathcal{Y}_i^g$ .

Similarly,  $\mathbb{P}_i^g(\mathcal{Y}_i^o \cup \mathcal{Y}_i^t \cup \mathcal{Y}_i^n)$  is the union of the convex quadrangles  $\mathbb{P}_i^g((n_r, n_c))$  for all  $(n_r, n_c) \in \mathcal{Y}_i^o \cup \mathcal{Y}_i^t \cup \mathcal{Y}_i^n$ .

## REFERENCES

- [1] Saif Salah Abood, Karim Qasim Hussein, and Methaq Talib Gaata. Survey on Modern Applications of Multiple Unmanned Aerial Vehicles (UAV) Systems. In *2022 Fifth College of Science International Conference of Recent Trends in Information Technology (CSCTIT)*, pages 179–184. IEEE, 2022.
- [2] Yug Ajmera and Surya Pratap Singh. Autonomous UAV-based Target Search, Tracking and Following using Reinforcement Learning and YOLOFlow. In *2020 IEEE International Symposium on Safety, Security, and Rescue Robotics (SSRR)*, pages 15–20. IEEE, 2020.
- [3] Bethany Allik. Tracking of multiple targets across distributed platforms with fov constraints. In *in Proc. IEEE CDC*, pages 6044–6049, 2019.
- [4] Arash Asgharivaskasi and Nikolay Atanasov. Semantic OcTree mapping and Shannon mutual information computation for robot exploration. *IEEE Transactions on Robotics*, 2023. Publisher: IEEE.
- [5] Nikolay Atanasov, Bharath Sankaran, Jerome Le Ny, George J Pappas, and Kostas Daniilidis. Nonmyopic view planning for active object classification and pose estimation. *IEEE Transactions on Robotics*, 30(5):1078–1090, 2014. Publisher: IEEE.

- [6] Arundhati Banerjee and Jeff Schneider. Decentralized Multi-Agent Active Search and Tracking when Targets Outnumber Agents. *arXiv preprint arXiv:2401.03154*, 2024.
- [7] Panagiotis D Christofides, Riccardo Scattolini, David Munoz De La Pena, and Jinfeng Liu. Distributed model predictive control: A tutorial review and future research directions. *Computers & Chemical Engineering*, 51:21–41, 2013.
- [8] ID Coope. Reliable computation of the points of intersection of  $n$  spheres in  $R^n$ . *ANZIAM Journal*, 42:C461–C477, 2000.
- [9] Philip M Dames. Distributed multi-target search and tracking using the PHD filter. *Autonomous robots*, 44(3):673–689, 2020.
- [10] Thiago Marchi Di Gennaro and Jacques Waldmann. Sensor Fusion with Asynchronous Decentralized Processing for 3D Target Tracking with a Wireless Camera Network. *Sensors*, 23(3):1194, 2023.
- [11] Zhaoxin Fan, Yazhi Zhu, Yulin He, Qi Sun, Hongyan Liu, and Jun He. Deep learning on monocular object pose detection and tracking: A comprehensive overview. *ACM Computing Surveys*, 55(4):1–40, 2022.
- [12] Olivier Faugeras. *Three-dimensional computer vision: a geometric viewpoint*. MIT press, 1993.
- [13] Alex Goldhoorn, Anaís Garrell, René Alquézar, and Alberto Sanfeliu. Searching and tracking people with cooperative mobile robots. *Autonomous Robots*, 42(4):739–759, 2018.
- [14] Eleonora Grilli, Fabio Menna, and Fabio Remondino. A review of point clouds segmentation and classification algorithms. *The International Archives of Photogrammetry, Remote Sensing and Spatial Information Sciences*, 42:339, 2017. Publisher: Copernicus GmbH.
- [15] Guillaume Hardouin, Julien Moras, Fabio Morbidi, Julien Marzat, and El Mustapha Mouaddib. Next-Best-View planning for surface reconstruction of large-scale 3D environments with multiple UAVs. In *2020 IEEE/RSJ International Conference on Intelligent Robots and Systems (IROS)*, pages 1567–1574. IEEE, 2020.
- [16] Yukai Hou, Jin Zhao, Rongqing Zhang, Xiang Cheng, and Liuqing Yang. UAV Swarm Cooperative Target Search: A Multi-Agent Reinforcement Learning Approach. *IEEE Transactions on Intelligent Vehicles*, 2023.
- [17] Andrew Howard, Mark Sandler, Grace Chu, Liang-Chieh Chen, Bo Chen, Mingxing Tan, Weijun Wang, Yukun Zhu, Ruoming Pang, Vijay Vasudevan, and others. Searching for mobilenetv3. In *Proceedings of the IEEE/CVF international conference on computer vision*, pages 1314–1324, 2019.
- [18] Julius Ibenthal, Michel Kieffer, Luc Meyer, Hélène Piet-Lahanier, and Sébastien Reynaud. Bounded-error target localization and tracking using a fleet of UAVs. *Automatica*, 132:109809, 2021.
- [19] Julius Ibenthal, Luc Meyer, Helene Piet-Lahanier, and Michel Kieffer. Localization of Partially Hidden Moving Targets Using a Fleet of UAVs via Bounded-Error Estimation. *IEEE Transactions on Robotics*, 2023.
- [20] Luc Jaulin, Michel Kieffer, Olivier Didrit, and Eric Walter. *Applied Interval analysis*. Springer, 2001.
- [21] Hae-Gon Jeon, Jaesik Park, Gyeongmin Choe, Jinsun Park, Yunsu Bok, Yu-Wing Tai, and In So Kweon. Accurate depth map estimation from a lenslet light field camera. In *IEEE CVPR*, 2015.
- [22] Yatai Ji, Yong Zhao, Bin Chen, Zhengqiu Zhu, Yu Liu, Hai Zhu, and Sihang Qiu. Source searching in unknown obstructed environments through source estimation, target determination, and path planning. *Building and Environment*, 221:109266, 2022.
- [23] Peiyuan Jiang, Daji Ergu, Fangyao Liu, Ying Cai, and Bo Ma. A Review of Yolo algorithm developments. *Procedia computer science*, 199:1066–1073, 2022.
- [24] Michael J Kuhlman, Michael W Otte, Donald Sofge, and Satyandra K Gupta. Multipass target search in natural environments. *Sensors*, 2017.
- [25] Mikko Lauri, David Hsu, and Joni Pajarinen. Partially observable markov decision processes in robotics: A survey. *IEEE Transactions on Robotics*, 39(1):21–40, 2022. Publisher: IEEE.
- [26] Juan Li, Xiaoliang Zhai, Jian Xu, and Chengyue Li. Target search algorithm for AUV based on real-time perception maps in unknown environment. *Machines*, 2021.
- [27] Daqian Liu, Weidong Bao, Xiaomin Zhu, Bowen Fei, Zhenliang Xiao, and Tong Men. Vision-aware air-ground cooperative target localization for UAV and UGV. *Aerospace Science and Technology*, 124:107525, 2022.
- [28] Yisha Liu, Qunxiang Wang, Huosheng Hu, and Yuqing He. A novel real-time moving target tracking and path planning system for a quadrotor UAV in unknown unstructured outdoor scenes. *IEEE Transactions on Systems, Man, and Cybernetics: Systems*, 49(11):2362–2372, 2018.
- [29] Yuting Liu, Manman Xu, Guozhang Jiang, Xiliang Tong, Juntong Yun, Ying Liu, Baojia Chen, Yongcheng Cao, Nannan Sun, and Zeshen Li. Target localization in local dense mapping using RGBD SLAM and object detection. *Concurrency and Computation: Practice and Experience*, 34(4):e6655, 2022. Publisher: Wiley Online Library.
- [30] Xudong Luo, Yiquan Wu, and Langyue Zhao. YOLOD: A target detection method for UAV aerial imagery. *Remote Sensing*, 14(14):3240, 2022.
- [31] Mingyang Lyu, Yibo Zhao, Chao Huang, and Hailong Huang. Unmanned aerial vehicles for search and rescue: A survey. *Remote Sensing*, 15(13):3266, 2023.
- [32] Logambal Madhuanand, Francesco Nex, and Michael Ying Yang. Self-supervised monocular depth estimation from oblique UAV videos. *ISPRS journal of photogrammetry and remote sensing*, 2021.
- [33] Ajith Anil Meera, Marija Popovic, Alexander Millane, and Roland Siegwart. Obstacle-aware adaptive informative path planning for uav-based target search. In *in Proc. IEEE ICRA*, pages 718–724, 2019.
- [34] Shervin Minaee, Yuri Boykov, Fatih Porikli, Antonio Plaza, Nasser Kehtarnavaz, and Demetri Terzopoulos. Image segmentation using deep learning: A survey. *IEEE Trans Pattern Anal Mach Intell*, 44(7):3523–3542, 2021.
- [35] Sara Minaeian, Jian Liu, and Young-Jun Son. Vision-based target detection and localization via a team of cooperative UAV and UGVs. *IEEE Transactions on systems, man, and cybernetics: systems*, 2015.
- [36] Sara Minaeian, Jian Liu, and Young-Jun Son. Effective and efficient detection of moving targets from a UAV camera. *IEEE transactions on intelligent transportation systems*, 19(2):497–506, 2018. Publisher: IEEE.
- [37] Arsalan Mousavian, Dragomir Anguelov, John Flynn, and Jana Kosecka. 3d bounding box estimation using deep learning and geometry. In *Proceedings of the IEEE conference on Computer Vision and Pattern Recognition*, pages 7074–7082, 2017.
- [38] Tomasz Niedzielski, Mirosława Jurecka, Bartłomiej Mizinski, Wojciech Pawul, and Tomasz Motyl. First successful rescue of a lost person using the human detection system: A case study from Beskid Niski (SE Poland). *Remote Sensing*, 13(23):4903, 2021. Publisher: MDPI.
- [39] Jongho Park and Youdan Kim. Stereo vision based collision avoidance of quadrotor UAV. In *2012 12th International Conference on Control, Automation and Systems*, pages 173–178. IEEE, 2012.
- [40] Julio A Placed, Jared Strader, Henry Carrillo, Nikolay Atanasov, Vadim Indelman, Luca Carlone, and José A Castellanos. A survey on active simultaneous localization and mapping: State of the art and new frontiers. *IEEE Transactions on Robotics*, 2023.
- [41] Jorge Pena Queralt, Jussi Taipalmaa, Bilge Can Pullinen, Victor Kathan Sarker, Tuan Nguyen Gia, Hannu Tenhunen, Moncef Gabbouj, Jenni Raitoharju, and Tomi Westerlund. Collaborative multi-robot search and rescue: Planning, coordination, perception, and active vision. *Ieee Access*, 2020.
- [42] Léon Reboul, Michel Kieffer, Hélène Piet-Lahanier, and Sébastien Reynaud. Cooperative guidance of a fleet of UAVs for multi-target discovery and tracking in presence of obstacles using a set membership approach. *IFAC-PapersOnLine*, 52(12):340–345, 2019.
- [43] Joseph Redmon, Santosh Divvala, Ross Girshick, and Ali Farhadi. You only look once: Unified, real-time object detection. In *Proceedings of the IEEE conference on computer vision and pattern recognition*, pages 779–788, 2016.
- [44] Cyril Robin and Simon Lacroix. Multi-robot target detection and tracking: taxonomy and survey. *Autonomous Robots*, 40(4):729–760, 2016. Number: 4 Publisher: Springer.
- [45] Caner Sahin, Guillermo Garcia-Hernando, Juil Sock, and Tae-Kyun Kim. A review on object pose recovery: from 3d bounding box detectors to full 6d pose estimators. *Image and Vision Computing*, 96:103898, 2020. Publisher: Elsevier.
- [46] Quentin Serdel, Julien Marzat, and Julien Moras. SMA<sub>Na</sub>: Semantic Mapping and Navigation Architecture for Autonomous Robots. 2023.
- [47] Tomoyasu Shimada, Hiroki Nishikawa, Xiangbo Kong, and Hiroyuki Tomiyama. Fast and High-Quality Monocular Depth Estimation with Optical Flow for Autonomous Drones. *Drones*, 2023.
- [48] Amarjeet Singh, Fabio Ramos, Hugh Durrant Whyte, and William J Kaiser. Modeling and decision making in spatio-temporal processes for environmental surveillance. In *2010 IEEE International Conference on Robotics and Automation*, pages 5490–5497. IEEE, 2010.
- [49] Jingxuan Sun, Boyang Li, Yifan Jiang, and Chih-yung Wen. A camera-based target detection and positioning UAV system for search and rescue (SAR) purposes. *Sensors*, 16(11):1778, 2016. Publisher: MDPI.
- [50] Andrew Symington, Sonia Waharte, Simon Julier, and Niki Trigoni. Probabilistic target detection by camera-equipped UAVs. In *in Proc. IEEE ICRA*, pages 4076–4081, 2010.
- [51] Hongwei Tang, Wei Sun, Hongshan Yu, Anping Lin, Min Xue, and Yuxue Song. A novel hybrid algorithm based on PSO and FOA for target

- searching in unknown environments. *Applied Intelligence*, 49:2603–2622, 2019. Publisher: Springer.
- [52] Fernando Vanegas, Duncan Campbell, Markus Eich, and Felipe Gonzalez. UAV based target finding and tracking in GPS-denied and cluttered environments. In *2016 IEEE/RSJ International Conference on Intelligent Robots and Systems (IROS)*, pages 2307–2313. IEEE, 2016.
- [53] Xuan Wang, Jinghong Liu, and Qianfei Zhou. Real-time multi-target localization from unmanned aerial vehicles. *Sensors*, 17(1):33, 2016. Number: 1 Publisher: MDPI.
- [54] Evsen Yanmaz. Joint or decoupled optimization: Multi-UAV path planning for search and rescue. *Ad Hoc Networks*, 138:103018, 2023. Publisher: Elsevier.
- [55] Zhen Zeng, Yunwen Zhou, Odest Chadwicke Jenkins, and Karthik Desingh. Semantic mapping with simultaneous object detection and localization. In *RSJ International Conference on Intelligent Robots and Systems (IROS)*, pages 911–918, 2018.
- [56] Boquan Zhang, Xiang Lin, Yifan Zhu, JING Tian, and Zhi Zhu. Enhancing Multi-UAV Reconnaissance and Search Through Double Critic DDPG With Belief Probability Maps. *IEEE Trans. Intell. Veh.*, 2024.
- [57] Haihan Zhang, Chun Xie, Hisatoshi Toriya, Hidehiko Shishido, and Itaru Kitahara. Vehicle Localization in a Completed City-Scale 3D Scene Using Aerial Images and an On-Board Stereo Camera. *Remote Sensing*, 15(15):3871, 2023. Publisher: MDPI.
- [58] Shiyong Zhang, Xuebo Zhang, Tianyi Li, Jing Yuan, and Yongchun Fang. Fast active aerial exploration for traversable path finding of ground robots in unknown environments. *IEEE Transactions on Instrumentation and Measurement*, 71:1–13, 2022. Publisher: IEEE.
- [59] Lei Zhao, Rui Li, Jianda Han, and Jianlei Zhang. A distributed model predictive control-based method for multidifferent-target search in unknown environments. *IEEE Trans. Evol. Comput.*, 27(1):111–125, 2022.
- [60] Ziyang Zhen, Yan Chen, Liangdong Wen, and Bing Han. An intelligent cooperative mission planning scheme of UAV swarm in uncertain dynamic environment. *Aerospace Science and Technology*, 100:105826, 2020. Publisher: Elsevier.
- [61] Fangwei Zhong, Sheng Wang, Ziqi Zhang, and Yizhou Wang. Detect-SLAM: Making object detection and SLAM mutually beneficial. In *2018 IEEE Winter Conference on Applications of Computer Vision (WACV)*, pages 1001–1010. IEEE, 2018.
- [62] Xiaolong Zhu, Fernando Vanegas, Felipe Gonzalez, and Conrad Sanderson. A Multi-UAV System for Exploration and Target Finding in Cluttered and GPS-Denied Environments. In *Proc. IEEE ICUAS*, 2021.